AD-A113 903 PENNSYLVANIA STATE UNIV UNIVERSITY PARK APPLIED RESE--ETC F/G 7/4
DIFFRACTION EFFECTS OF APERTURES IN THE EXTREME NEARFIELD.(U)
FEB 82 R L OCHS N00024-79-C-6043
UNCLASSIFIED ARL/PSU/TM-82-70 NL

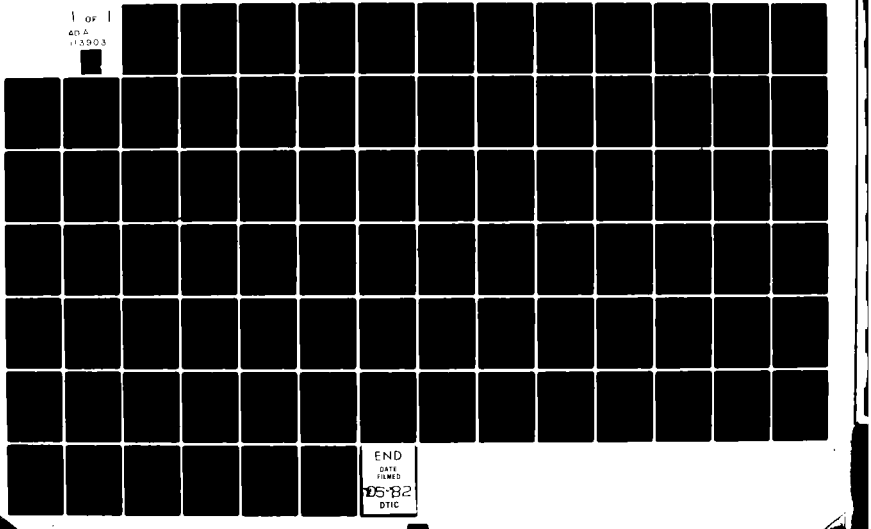

(5)

DIFFRACTION EFFECTS OF APERTURES IN THE EXTREME NEARFIELD

Robert L. Ochs, Jr.

Technical Memorandum
File No. TM 82-70
February 12, 1982
Contract No. N00024-79-C-6043

Copy No. 5

The Pennsylvania State University
Intercollege Research Programs and Facilities
APPLIED RESEARCH LABORATORY
Post Office Box 30
State College, PA 16801

NAVY DEPARTMENT

NAVAL SEA SYSTEMS COMMAND

REPORT DOCUMENTATION PAGE

READ INSTRUCTIONS BEFORE COMPLETING FORM

1. REPORT NUMBER: TM 82-70	2. GOVT ACCESSION NO.: AD-A113903
3. RECIPIENT'S CATALOG NUMBER	
4. TITLE (and Subtitle): DIFFRACTION EFFECTS OF APERTURES IN THE EXTREME NEARFIELD	5. TYPE OF REPORT & PERIOD COVERED: M.S. Thesis, May 1982
	6. PERFORMING ORG. REPORT NUMBER: TM 82-70
7. AUTHOR(s): Robert L. Ochs, Jr.	8. CONTRACT OR GRANT NUMBER(s): N00024-79-C-6043
9. PERFORMING ORGANIZATION NAME AND ADDRESS: The Pennsylvania State University, Applied Research Laboratory, P.O. Box 30, State College, PA 16801	10. PROGRAM ELEMENT, PROJECT, TASK AREA & WORK UNIT NUMBERS
11. CONTROLLING OFFICE NAME AND ADDRESS: Naval Sea Systems Command, Department of the Navy, Washington, DC 20362	12. REPORT DATE: February 12, 1982
	13. NUMBER OF PAGES: 74 Pages & figures
14. MONITORING AGENCY NAME & ADDRESS (if different from Controlling Office)	15. SECURITY CLASS. (of this report): Unclassified, Unlimited
	15a. DECLASSIFICATION/DOWNGRADING SCHEDULE

16. DISTRIBUTION STATEMENT (of this Report)

Approved for public release, distribution unlimited, per NSSC (Naval Sea Systems Command), 6/23/81.

17. DISTRIBUTION STATEMENT (of the abstract entered in Block 20, if different from Report)

18. SUPPLEMENTARY NOTES

19. KEY WORDS (Continue on reverse side if necessary and identify by block number)

sound, field, apertures, diffraction, near field, thesis

20. ABSTRACT (Continue on reverse side if necessary and identify by block number)

A model is developed that describes, at least qualitatively, the sound field within a wavelength of an aperture in an opaque, plane screen insonified by harmonic waves. The normal component of the particle velocity is assumed to be the same in the aperture as if no screen were present and zero everywhere else in the plane of the screen. Using this assumption, an expression for the transmitted sound field is developed in the form of the inverse Fourier transform of the product of the Fourier transform of the normal component of the particle velocity in the plane of the screen and the Fourier transform of

the Green function appropriate for Neumann boundary conditions on a plane. This expression can be evaluated quickly using a fast-Fourier-transform (FFT) algorithm. The validity of the above assumption is demonstrated in the extreme nearfield by comparison with experiment for the case of a diffraction grating of straight strips separated by a distance less than a wavelength and insonified by plane waves. The model is then used to study the diffraction of cylindrical waves by a grating of straight strips. A rapid method of calculating exactly the sound field of an oscillating piston of arbitrary configuration in a rigid baffle is also indicated.

Finally, a simple model is developed to calculate the extreme nearfield for points of observation on the axis of symmetry of an aperture consisting of concentric rings insonified by plane waves. It is shown that a significant focusing effect can be observed at distances within a wavelength of the aperture.

ABSTRACT

A model is developed that describes, at least qualitatively, the sound field within a wavelength of an aperture in an opaque, plane screen insonified by harmonic waves. The normal component of the particle velocity is assumed to be the same in the aperture as if no screen were present and zero everywhere else in the plane of the screen. Using this assumption, an expression for the transmitted sound field is developed in the form of the inverse Fourier transform of the product of the Fourier transform of the normal component of the particle velocity in the plane of the screen and the Fourier transform of the Green function appropriate for Neumann boundary conditions on a plane. This expression can be evaluated quickly using a fast-Fourier-transform (FFT) algorithm. The validity of the above assumption is demonstrated in the extreme nearfield by comparison with experiment for the case of a diffraction grating of straight strips separated by a distance less than a wavelength and insonified by plane waves. The model is then used to study the diffraction of cylindrical waves by a grating of straight strips. A rapid method of calculating exactly the sound field of an oscillating piston of arbitrary configuration in a rigid baffle is also indicated.

Finally, a simple model is developed to calculate the extreme nearfield for points of observation on the axis of symmetry of an aperture consisting of concentric rings insonified by plane waves. It is shown that a significant focusing effect can be observed at distances within a wavelength of the aperture.

TABLE OF CONTENTS

TABLE OF CONTENTS (continued)

LIST OF FIGURES

LIST OF FIGURES (continued)

LIST OF FIGURES (continued)

LIST OF FIGURES (continued)

LIST OF FIGURES (continued)

LIST OF FIGURES (continued)

ACKNOWLEDGEMENTS

The author wishes to express his gratitude to his thesis advisers, Dr. W. Jack Hughes and Professor J. D. Maynard, and to Drs. Earl G. Williams and Arthur D. Gorman for their advice and encouragement in the performance and documentation of this research. In addition, the author wishes to acknowledge the support of the Applied Research Laboratory of The Pennsylvania State University under contract with the Naval Sea Systems Command.

CHAPTER I

BACKGROUND AND OBJECTIVES

1.1 Introduction

A diffraction grating consists of an array of slits having a width comparable to the wavelength of the waves illuminating the grating. The illuminating radiation may be electromagnetic waves, acoustic waves, or may even consist of a stream of particles interpreted quantum mechanically. Recently an experiment was conducted to determine the effects of an acoustic diffraction grating placed very near (within a fraction of a wavelength) to a receive transducer. The results obtained could not be interpreted in terms of the usual Fraunhofer or Fresnel diffraction theories since these require that the observation point be at least several wavelengths from the grating. Other recent experiments [14] have shown that the extreme nearfield (within a fraction of a wavelength) of even the simplest sources can behave quite independently from what one would expect from observing only the customary nearfield (usually more than one wavelength away). In the research presented in this thesis, a simple numerical technique to calculate the nearfield of complex sound sources is used to develop a model for the diffraction grating observations. This model is then used to study the effect on the received sound radiation when the incident waves are no longer plane waves. Finally, a model is developed to evaluate the pressure at points on the axis of symmetry of a grating consisting of concentric rings.

1.2 Background

Prior to 1970 [16], the sound field of an oscillating, circular piston in an infinite baffle had remained, except for the solution of Stenzel [11], inadequately investigated for points of observation located at distances comparable to a wavelength and off the axis of symmetry of the piston. No accurate calculations of the nearfield have been performed for such fundamental problems as radiation from a rectangular piston or the analogous problem of diffraction of a plane wave through a rectangular aperture in an infinitely extended plane screen. For these problems, the most accurate calculations that can be readily performed usually include the standard approximations of Fresnel diffraction [3, 10, 15]. These approximate solutions thus lose validity for points of observation located at distances less than, or of the order of magnitude of, the width of the piston or aperture [3]. The reasons for these approximations are made apparent below.

Through the use of Green's theorem, it is possible to compute the sound field everywhere in a region of space given the sound pressure or its gradient on an enclosing surface. The resulting expression for the sound field in the volume of interest is in the form of a surface integral over the bounding surface; this integral is usually very difficult if not impossible to evaluate in closed form without making various approximations that simplify the form of the integral. When considering sound passing through an aperture in a plane screen or sound radiated by an oscillating piston in a rigid baffle, the approximation made in the Fresnel theory of diffraction is to assume

that the observation point is far from the aperture (or piston) compared to a distance comparable to the size of the aperture (or piston). In addition, when considering the diffraction of waves through an aperture, mathematically inconsistent values for the sound field and its normal derivative are assumed as boundary conditions (Kirchhoff boundary conditions). As can be seen from the date of the paper by Zemanek [16], it was not realized until rather late that one need not make such approximations if the above integral is to be evaluated by computer. All this was in spite of the fact that a need was demonstrated as early as 1958 [9] for precise knowledge of the extreme nearfield of a circular piston for use in ultrasonics in medicine.

1.3 Scope of this Work

In this thesis, it is shown that it is possible to study, at least qualitatively, the extreme nearfield (less than a wavelength) of an aperture in an opaque plane screen illuminated by sound waves where the primary working assumption is that the particle velocity in the aperture is the same as if no screen were present and zero everywhere else in the plane of the screen. Specifically, in Chapter II an expression for the sound field transmitted through an aperture of arbitrary configuration is derived for any incident, harmonic waveform. In Chapter III, the above expression is specialized to the case of a diffraction grating of slits comparable in width to the wavelength of the incident sound. To test the validity of the working assumption in the extreme nearfield, the results of computations

of the transmitted sound field for incident plane waves are compared with experiment. A diffraction grating insonified by cylindrical waves emitted from a line source parallel to the slits is also considered. In Chapter IV, a model is developed and predictions are made of the sound pressure on the axis of symmetry of an aperture consisting of an array of concentric rings in an infinite baffle. Finally, in Chapter V a summary of the results of this study is presented, along with suggestions for future work. In addition, it is pointed out that the technique developed in Chapter II allows rapid and accurate calculation without approximation of the extreme nearfield of an oscillating piston or planar complex vibrator of any configuration in a rigid baffle.

CHAPTER II

DEVELOPMENT OF THE GENERAL SOLUTION

2.1 Introduction

In this chapter a general expression is derived for the sound field transmitted through an aperture in an infinite, opaque screen for harmonic waves incident from the side of the screen opposite to the point of observation. It is assumed that the particle velocity in the aperture is the same as if no screen were present and zero everywhere else in the plane of the screen. The limitations of this assumption are discussed in Chapter III.

2.2 Solution

Consider an aperture in an opaque screen of infinite extent located in the $z = 0$ plane of a rectangular coordinate system having axes x, y, and z. Let the point where the sound field is to be computed (observation point) have a z coordinate greater than zero. Let $\bar{u}_i(\bar{x},t)$ represent the particle velocity of the incident wave. If the incident wave is assumed to be an harmonic wave, then $\bar{u}_i(\bar{x},t) = \bar{u}_i(\bar{x})e^{-i\omega t}$. The factor $e^{-i\omega t}$ is hereafter neglected.

Employing the assumption that the particle velocity in the aperture is the same as if no screen were present and zero everywhere else in the $z = 0$ plane, we may write the z component of the particle velocity in the $z = 0$ plane as

$$u_z(x,y) = f(x,y)u_{i_z}(x,y,0) . \qquad (2.2.1)$$

f(x,y) is a function having the value one for all points (x,y,0) in the aperture and zero for all other points in the plane of the screen.

The pressure at any point (x,y,z>0) is known to be [5]

$$p(x,y,z) = -\int_{-\infty}^{\infty}\int_{-\infty}^{\infty} dx'dy' \frac{\partial p}{\partial z}, (x',y',0)G_N(x-x',y-y',z),$$

provided of course one can specify $\frac{\partial p}{\partial z}$ everywhere for z = 0. G_N is the Neumann Green function for the plane z = 0:

$$G_N(x,y,z) = \frac{e^{ik(x^2+y^2+z^2)^{\frac{1}{2}}}}{2\pi(x^2+y^2+z^2)^{\frac{1}{2}}} . \qquad (2.2.2)$$

k is a constant equal to ω/c for plane waves. Using the relation [8]

$$\bar{u}(\bar{x}) = \frac{1}{i\omega\rho} \bar{\nabla} p(\bar{x})$$

connecting the particle velocity of an harmonic sound wave with the pressure, we have

$$p(x,y,z) = -i\omega\rho \int_{-\infty}^{\infty}\int_{-\infty}^{\infty} dx'dy' \; u_z(x',y')G_N(x-x',y-y',z).$$

For constant z , this expression is in the form of a convolution integral. Thus, denoting the two-dimensional Fourier transform [8] by F_2 and the inverse Fourier transform by F_2^{-1}, we develop the following expression for the pressure:

$$p(x,y,z) = -i\omega\rho F_2^{-1}[F_2(u_z)F_2(G_N)]. \qquad (2.2.3)$$

The two-dimensional Fourier transform of $G_N(x,y,z)$ can be written in closed form as (Appendix A)

$$F_2(G_N) = G_N(k_x,k_y,z) = \begin{cases} \dfrac{i \exp[iz(k^2-k_x^2-k_y^2)^{\frac{1}{2}}]}{(k^2-k_x^2-k_y^2)^{\frac{1}{2}}}, & 0<k_x^2+k_y^2<k^2, z>0 \\ \dfrac{\exp[-z(k_x^2+k_y^2-k^2)^{\frac{1}{2}}]}{(k_x^2+k_y^2-k^2)^{\frac{1}{2}}}, & 0<k^2<k_x^2+k_y^2, z>0. \end{cases} \tag{2.2.4}$$

A general expression for $F_2(u_z)$ does not exist as it depends on the geometry of the aperture, through $f(x,y)$, and on the incident waveform, through $u_{i_z}(x,y,0)$.

CHAPTER III

GRATING OF PARALLEL SLITS

3.1 Introduction

Because no general expression exists for the two-dimensional Fourier transform of Equation (2.2.1), it must be evaluated for each aperture geometry and incident waveform considered. In this chapter, an expression for the transform of Equation (2.2.1) is written for the case of plane waves and cylindrical waves incident on a grating of a finite number of infinitely long, parallel slits. A simplified form of Equation (2.2.3) is then evaluated numerically for both plane waves and cylindrical waves. The results of these computations, for incident plane waves, are compared with experiment.

3.2 Incident Plane Waves

3.2.1 Expression for the transmitted sound field. Consider a finite number of slits of width a and infinite length in an opaque screen of infinite extent placed symmetrically in the $z = 0$ plane of a rectangular coordinate system. Let the edges of the slits be parallel to the y axis and separated by a width b of screen, as in Figure 1.

For a plane wave incident from below the grating, having a wave vector $\bar{k}$ perpendicular to the y axis, and making an angle θ with respect to the z axis as in Figure 1, Equation (2.2.1) becomes

$$u_z(x,y) = u_o f(x) \exp[i(2\pi/\lambda)\, x \sin\theta] \cos\theta,$$

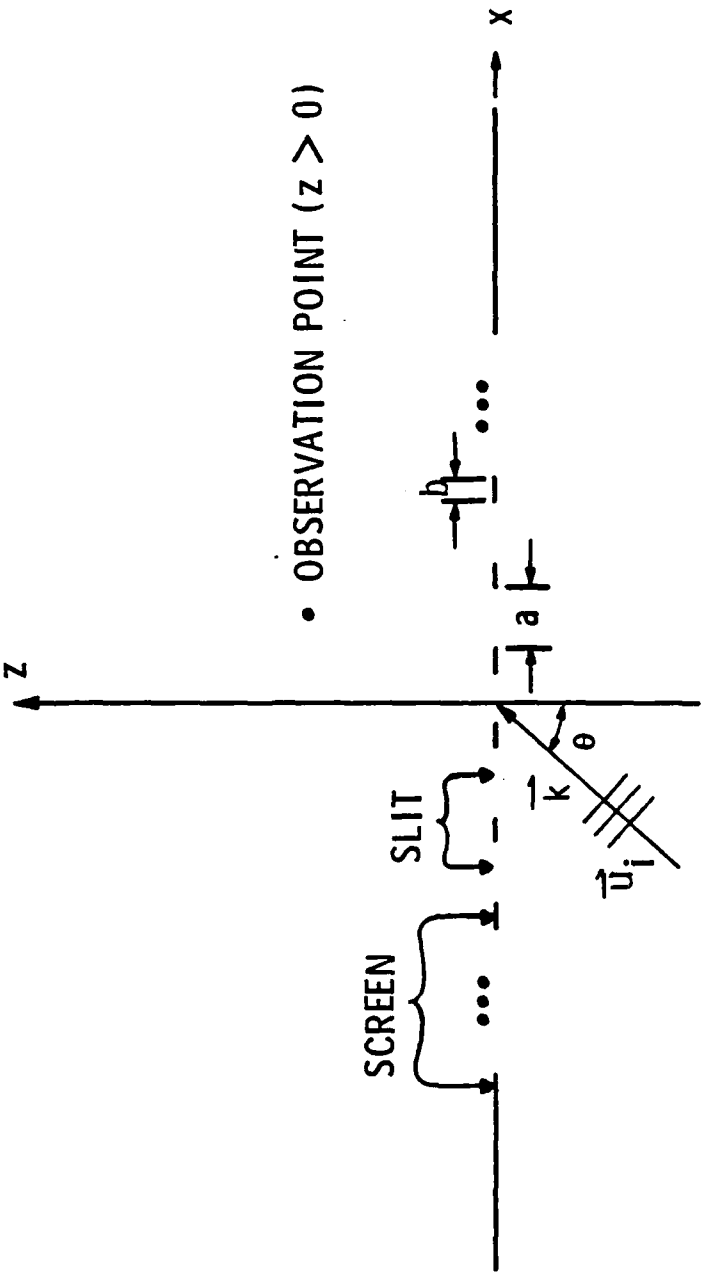

Figure 1. Reference geometry for incident plane waves.

where u_o is the amplitude of the particle velocity of the incident plane wave, $k = |\bar{k}| = 2\pi/\lambda$, and $f(x)$ is a function having the value one for all points $(x,y,0)$ in the slits and zero for all other points in the plane of the grating. After lengthy but straightforward calculation, the two-dimensional Fourier transform of $u_z(x,y)$ is found to be

$$F_2(u_z) = \frac{4\pi u_o \cos\theta\, \delta(k_y) \sin[(\frac{2\pi}{\lambda}\sin\theta - k_x)\frac{a}{2}] \sin[n(\frac{2\pi}{\lambda}\sin\theta - k_x)(\frac{a+b}{2})]}{(\frac{2\pi}{\lambda}\sin\theta - k_x)\sin[(\frac{2\pi}{\lambda}\sin\theta - k_x)(\frac{a+b}{2})]},$$

where n is the number of slits. The delta function arises from the infinite extent of the slits in the positive and negative y directions.

Thus, $F_2(u_z) = 2\pi\delta(k_y)u_z(k_x)$ where

$$u_z(k_x) = \frac{2u_o \cos\theta\, \sin[(\frac{2\pi}{\lambda}\sin\theta - k_x)\frac{a}{2}] \sin[n(\frac{2\pi}{\lambda}\sin\theta - k_x)(\frac{a+b}{2})]}{(\frac{2\pi}{\lambda}\sin\theta - k_x)\sin[(\frac{2\pi}{\lambda}\sin\theta - k_x)(\frac{a+b}{2})]}. \quad (3.2.1.1)$$

Finally, substituting the above expression into Equation (2.2.3) we obtain the result

$$p(x,z) = -i\omega\rho F_1^{-1}\,[u_z(k_x)\, G_N(k_x,0,z)], \quad (3.2.1.2)$$

where F_1^{-1} denotes the one-dimensional inverse Fourier transform.

3.2.2 Evaluation on a digital computer. Equation (3.2.1.2) was evaluated using a standard 256-point fast-Fourier-transform (FFT) algorithm. For all cases considered in this chapter, the Nyquist rate of two samples per wavelength was satisfied.

An FFT algorithm was chosen to evaluate Equation (3.2.1.2) because the number of arithmetic operations required is approximately $N \log_2 N$ as compared with N^2 operations required for the direct integral evaluation of Equation (3.2.1.2), where N is the number of integration points [2]. For N=256, this results in a factor of 30 savings in computer processing time compared to the time required for a direct integral evaluation of Equation (3.2.1.2).

It should be noted that as the distance z of the point of observation from the screen increases, the frequency of oscillation of $G_N(k_x,k_y,z)$, in the transform space, increases for $0<k_x^2+k_y^2<k^2$. As z becomes large it becomes increasingly difficult to satisfy the criterion expressed in the Nyquist rate theorem and, thus, aliasing becomes a significant problem. Aliasing also arises if the width a of the slits becomes very small as is obvious from Equation (3.2.1.1), which for $\theta=0$ is merely the Fraunhofer diffraction pattern for a grating of n slits [1]. Hence, if one wishes to study the transmitted sound field far from the grating or consider a grating of very narrow slits, an FFT algorithm having a large number of integration points must be used.

3.2.3 Brief description of an experiment. Before presenting the results of the numerical evaluation of Equation (3.2.1.2), we consider

briefly an experiment the results of which can be compared with calculated results.

An experiment was performed at the Applied Research Laboratory of The Pennsylvania State University by W. Jack Hughes in which the effects of a diffraction grating placed within a wavelength of a receive transducer were studied. An LC-10 hydrophone having an omnidirectional directivity pattern in isolation was placed symmetrically behind and 0.375 inches away from a diffraction grating consisting of sixteen styrofoam strips. Styrofoam was selected because it is a low ρc material and thereby acts as an opaque screen. The strips were 3/8 inches square, two feet long, and were carefully placed parallel to each other and 1.5 inches apart, as in Figure 2. Both the hydrophone and grating were suspended, in water, in the far-field of a projector such that the waves incident on the grating were plane to a good approximation. The graphs in Figures 3 and 4 of the experimentally measured pressure at the hydrophone as a function of the angle of incidence of the incident plane waves were obtained by rotating the grating about the axis of the hydrophone. The data in Figures 3 and 4 are normalized with respect to the pressure measured when no grating is present in the vicinity of the hydrophone.

3.2.4 Modeling of experimental results and comparison with experiment. To model the experimental situation, fifteen parallel slits 1.125 inches wide and infinitely long are considered, each slit being separated by 0.375 inches of screen. The point of observation is assumed to be 0.375 inches from the screen and centered directly behind the center slit (i.e., at (0,0,0.375) for a grating symmetri-

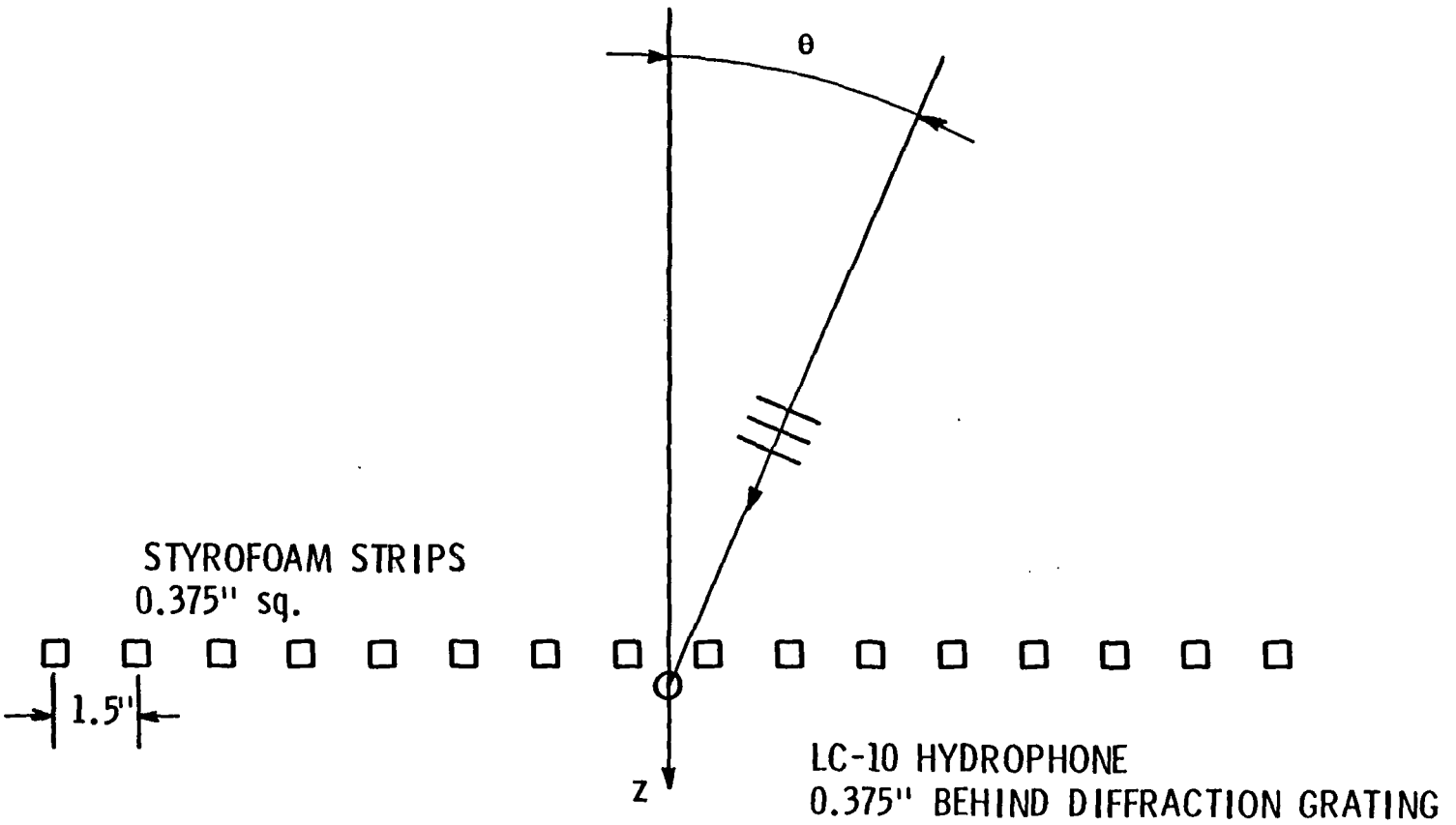

Figure 2. Experimental test set up for the acoustic diffraction grating.

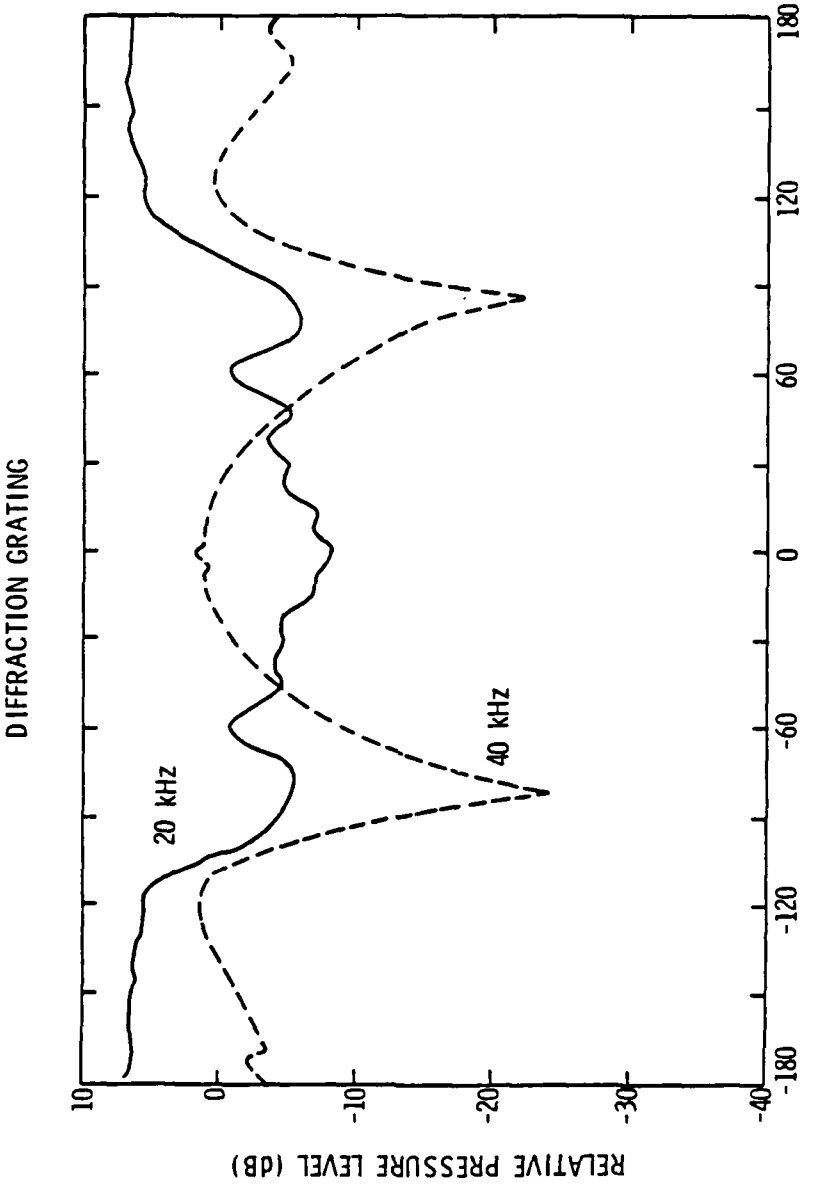

Figure 3. Experimentally measured directivity patterns at frequencies of 20 kHz (half wavelength spacing) and 40 kHz (full wavelength spacing).

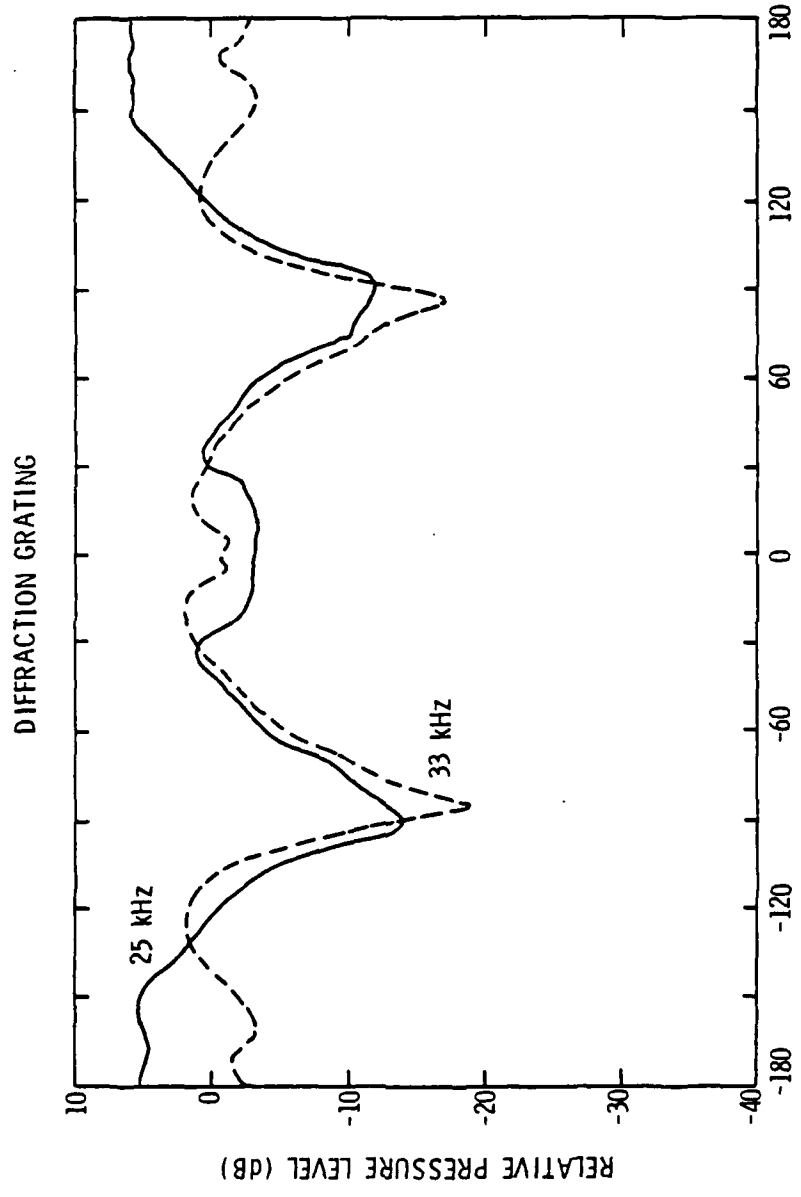

Figure 4. Experimentally measured directivity patterns at frequencies of 25 kHz and 33 kHz.

cally placed in the z = 0 plane and insonified from the negative z direction). The grating is assumed to be insonified by a plane wave, and the passage of sound around the grating as a whole is neglected, as though the slits were in a rigid screen of infinite extent. Also, the particle velocity in the slits is assumed to be the same as if no screen were present and zero everywhere else in the plane of the grating. To take into account in a simple manner the non-zero extent of the styrofoam strips in the direction normal to the grating, a geometrical analysis is performed to determine the pressure measured at the point of observation in the high frequency limit. In order to perform such an analysis, a scaled drawing of the experimental apparatus is constructed with the hydrophone positioned as shown in Figure 2. If the pressure measured by the hydrophone is assumed to be approximately proportional to the insonified area of the hydrophone normal to the direction of the incident sound ($dP \propto |\overline{k} \cdot \overline{dA}|$, where P is the pressure measured and $\overline{dA}$ is a vector perpendicular to the surface of the hydrophone), then the solid curve in Figure 5 is obtained. As can be seen from the solid curve, the calculated pressure curve (in dB) in the high frequency limit as a function of the angle of incidence (hereafter called a directivity pattern) has roughly the shape of a parabola for angles of incidence between -90° and +90°. Thus, to the directivity pattern obtained from the evaluation of Equation (3.2.1.2), a parabola of the form $\alpha\theta^2$ (in dB) is added, where $\alpha(dB/deg^2)$ is a negative parameter adjusted to best fit the experimental data.

The directivity patterns obtained using this semi-empirical model are compared with the experimentally obtained directivity patterns

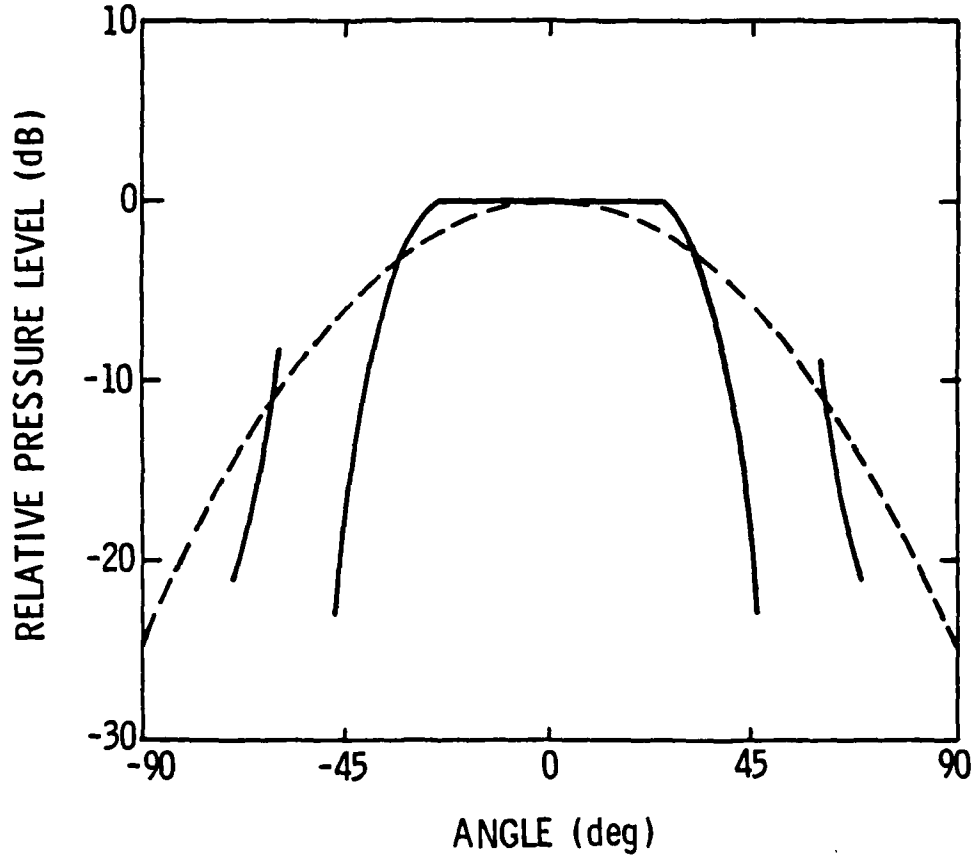

Figure 5. Calculated directivity pattern in the high frequency limit (solid curve) and the parabola $\alpha\theta^2$ for $\alpha = -30 \times 10^{-4}$(dashed curve).

in Figures 6, 7, and 8. The graph of α as a function of frequency in Figure 9 indicates that, as expected, α decreases in magnitude as the wavelength increases. The dashed curve in Figure 5 represents the parabola $\alpha\theta^2$ for α corresponding to a frequency of 40 kHz ($\alpha = -30\times10^{-4}$). As is apparent from Figures 6, 7, and 8, the agreement between theory and experiment is excellent for the frequencies considered. The deviation occurring at large angles is due in large part to the fact that in the experiment the hydrophone becomes directly insonified for large angles of incidence; this is not taken into account in the theory. This deviation decreases as the frequency increases, as expected.

It is extremely difficult to model the experimentally measured directivity pattern for plane waves incident at 20 kHz. The assumption made concerning the particle velocity in the plane of the grating, because it neglects interactions between slits and the precise mechanism of diffraction through a slit, apparently begins to produce a significant discrepancy between the experimental and calculated directivity patterns for frequencies below 25 kHz (0.625 wavelengths spacing between slits).

To gain physical insight into the experiment considered above, the model used to calculate the directivity patterns can be simplified by replacing the grating of fifteen slits by fifteen point sources distributed on a line and separated by 1.5 inches. The point sources must be properly phased to take into account the variation in the angle of incidence of the plane waves and a parabola $\alpha\theta^2$ must be added

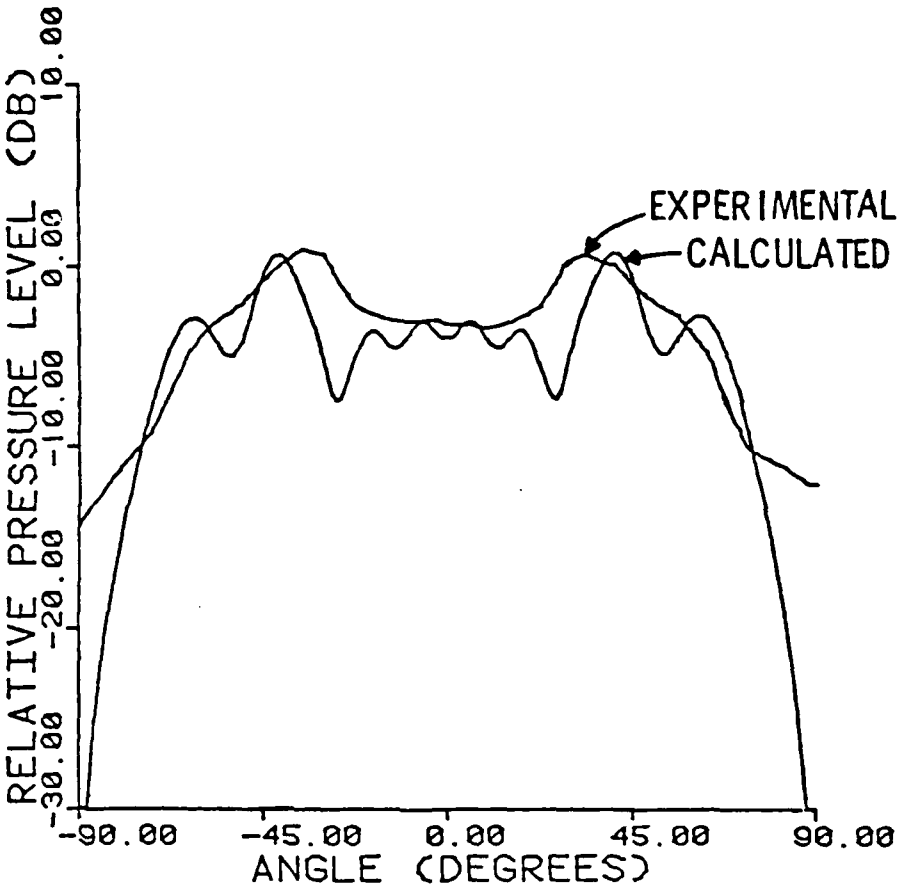

Figure 6. Experimental and calculated directivity patterns at 25 kHz (0.625 wavelengths spacing).

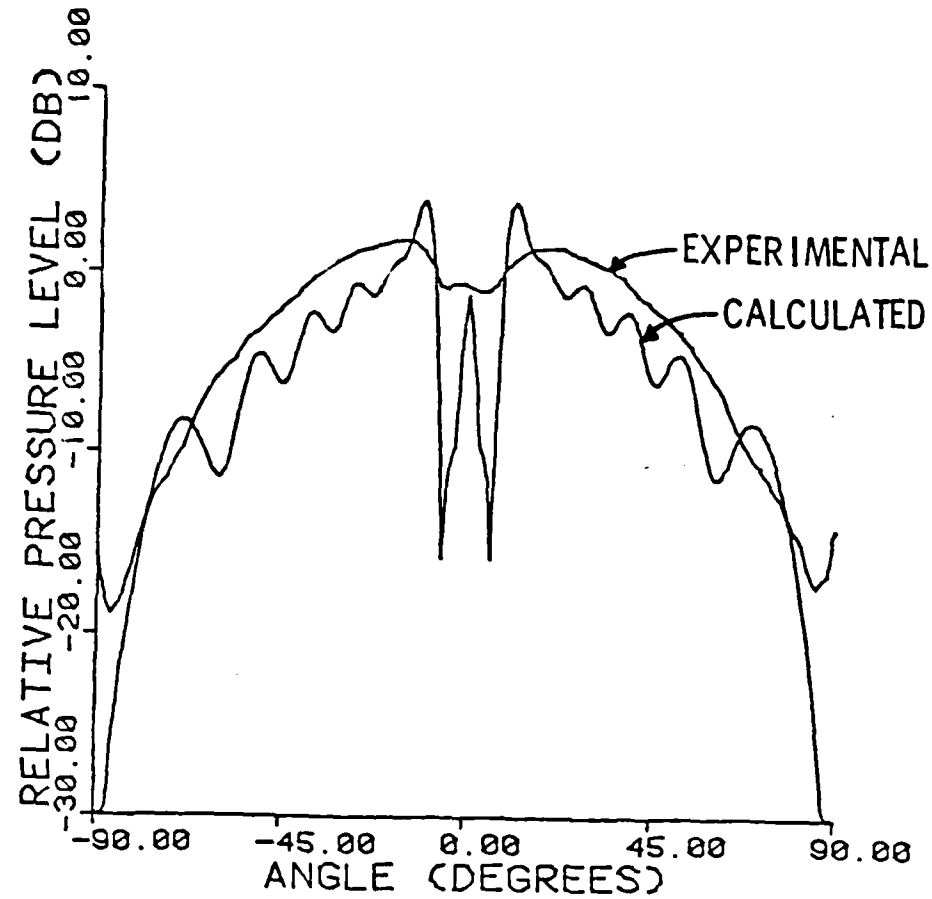

Figure 7. Experimental and calculated directivity patterns at 33 kHz (0.825 wavelengths spacing).

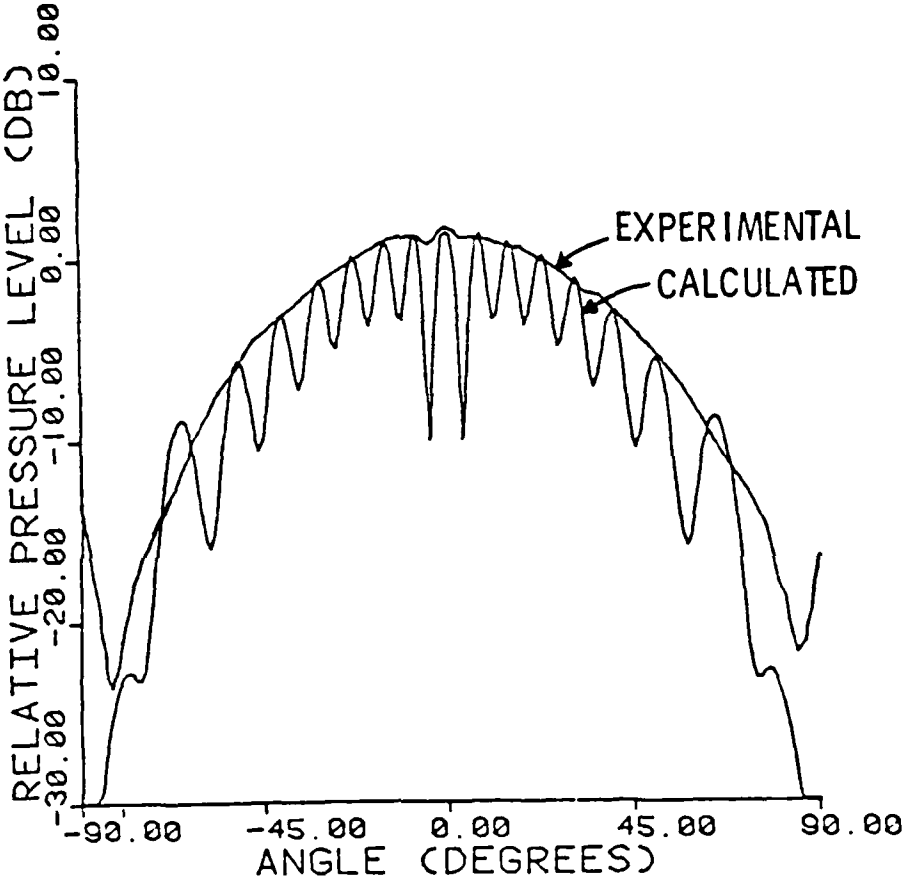

Figure 8. Experimental and calculated directivity patterns at 40 kHz (full wavelength spacing).

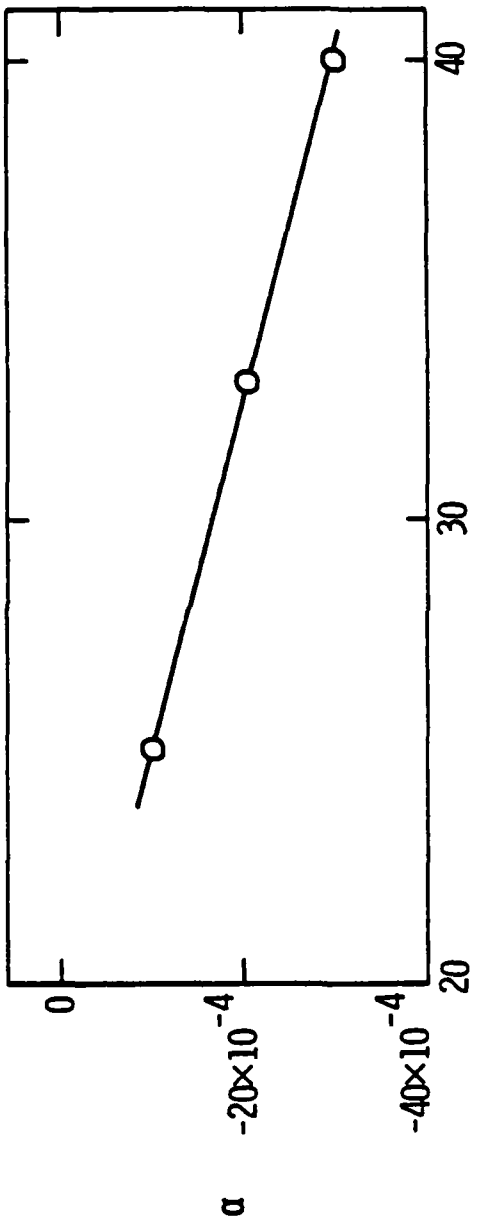

Figure 9. α as a function of frequency.

to the resulting directivity patterns, where α takes on the values given in Figure 9. The directivity patterns obtained from this model are in fairly good accord with experiment. If one replaces the styrofoam strips by 16 point sources separated by 1.5 inches as opposed to replacing the slits by point sources, as done above, poor agreement with experiment is obtained. Hence, better agreement with experiment is obtained if one does not consider the styrofoam strips as re-radiation sources.

3.2.5 Further calculated results for incident plane waves. Before leaving this investigation of the transmission of plane waves through a diffraction grating, we consider the effects on the directivity pattern of moving the hydrophone from its position in Figure 2 to other positions beneath the grating and the effects of decreasing the number of slits in the grating. The grating is still assumed to be composed of strips extended 0.375 inches in the direction normal to the grating.

Directivity patterns for 40 kHz plane waves incident on a grating of 15 slits are presented in Figures 10, 11 and 12, for a hydrophone on the axis of symmetry of the grating (z axis) and 0.1 inches, 0.4 inches, and 0.7 inches, respectively, from the grating. For these patterns, α is assumed to remain constant (-30×10^{-4} at 40 kHz) because we are considering excursions of the point of observation from the grating less than the width of a slit. Justification for this and other assumptions concerning the effects of geometry on α is offered at the end of this subsection. Notice that as the distance of the hydrophone from the grating increases, the directivity

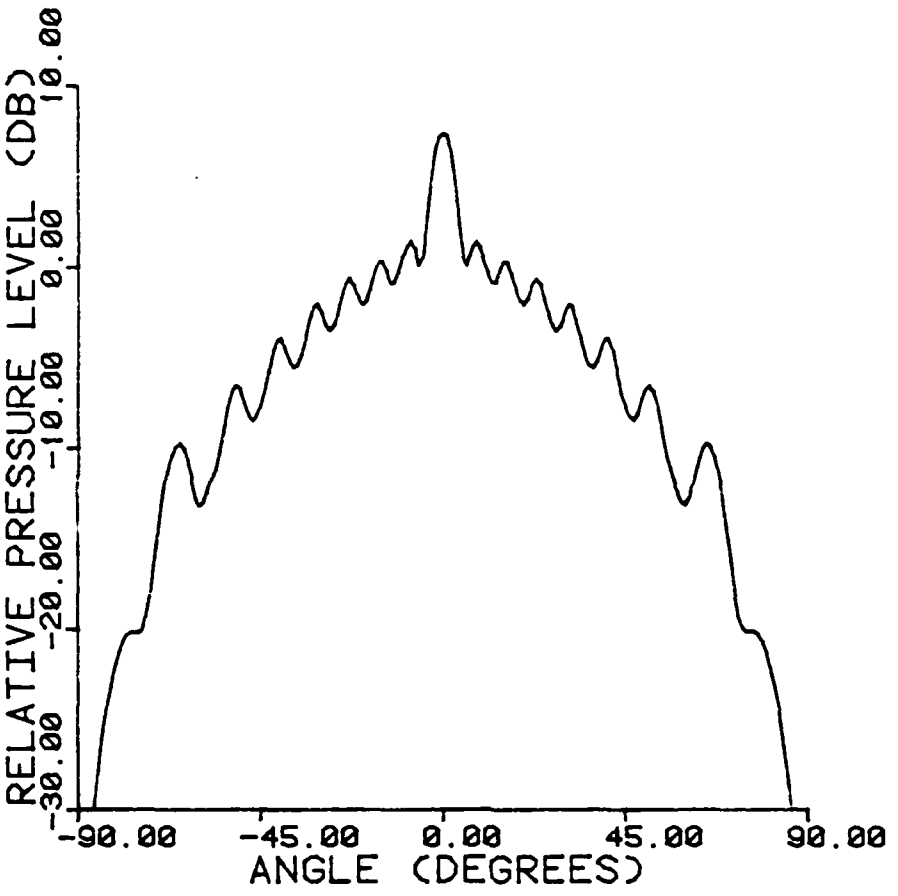

Figure 10. Calculated directivity pattern at 40 kHz for an LC-10 hydrophone 0.1" from a grating of 15 slits and on the axis of symmetry of the grating.

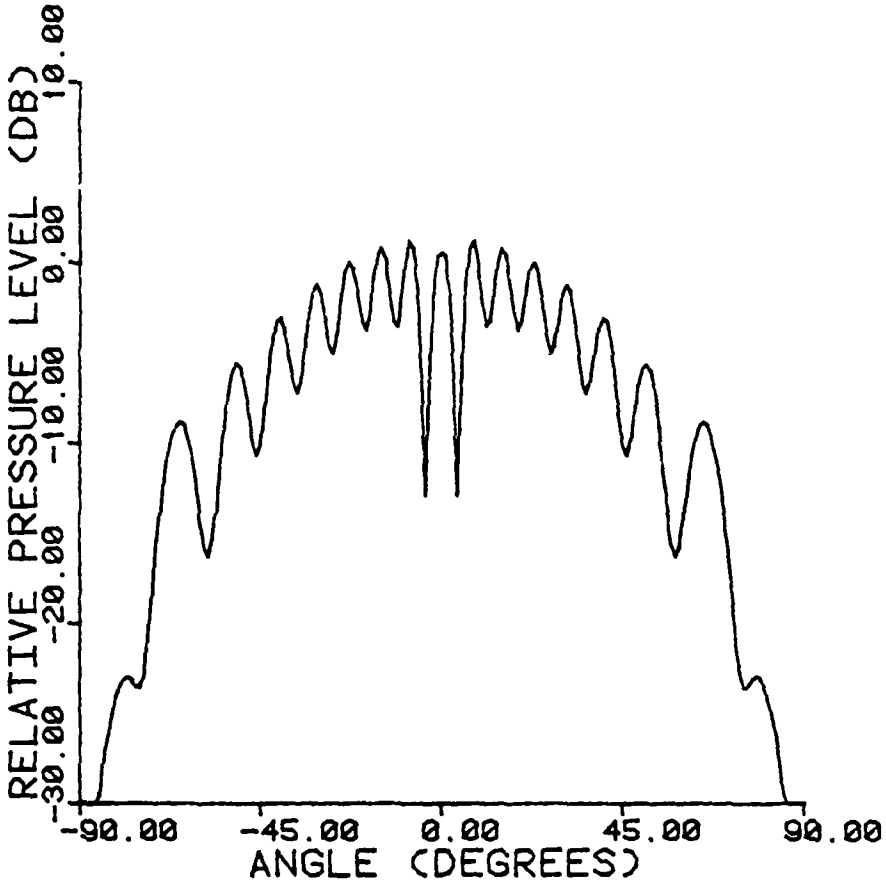

Figure 11. Calculated directivity pattern at 40 kHz for an LC-10 hydrophone 0.4" from a grating of 15 slits and on the axis of symmetry of the grating.

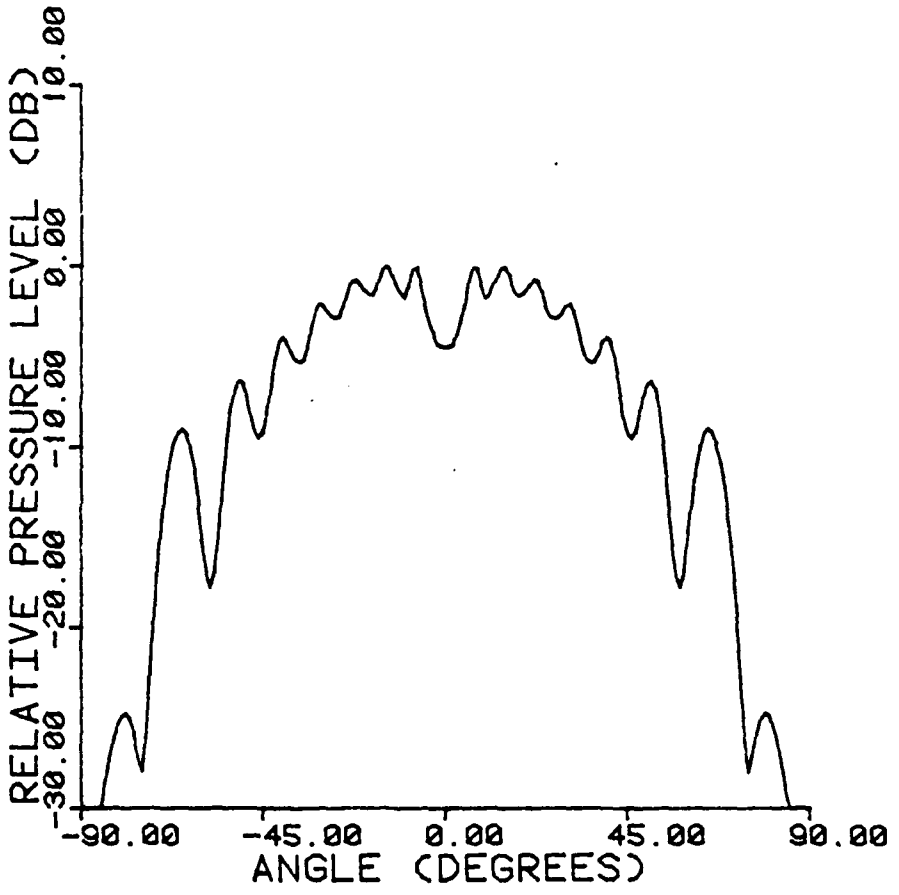

Figure 12. Calculated directivity pattern at 40 kHz for an LC-10 hydrophone 0.7" from a grating of 15 slits and on the axis of symmetry of the grating.

pattern at high angles remains relatively unchanged while the peak at $\theta=0°$ in Figure 10 drops to form a minimum at 0.7 inches from the grating.

In Figures 13, 14, and 15, keeping the hydrophone 0.375 inches away from the grating, directivity patterns are given illustrating the effects of moving the hydrophone from beneath a slit to beneath a styrofoam strip. α is assumed to decrease in magnitude linearly from its value beneath a slit (-30×10^{-4} at 40 kHz) to zero directly beneath a styrofoam strip. As expected, the patterns flatten and become asymmetrical as the point of observation moves off the axis of symmetry (z axis) towards a strip. Note the bright spot in the directivity pattern in Figure 15 for a hydrophone beneath a strip.

Finally, Figures 16, 17, 18, and 19 illustrate the effects on the directivity pattern of decreasing the number of slits in the grating for a hydrophone 0.375 inches from the grating and on the z axis. α is assumed to remain constant (-30×10^{-4} at 40 kHz) as the number of slits decreases. Of significance is the observation that forward directivity increases as the number of slits decreases despite the fact that α is the same in all four figures.

Implicit in Figures 10 through 19 are various assumptions concerning the effects of geometry on the parameter α, namely:

1. α remains approximately constant as the distance of the hydrophone from the grating changes provided the distance remains less than the width of a slit

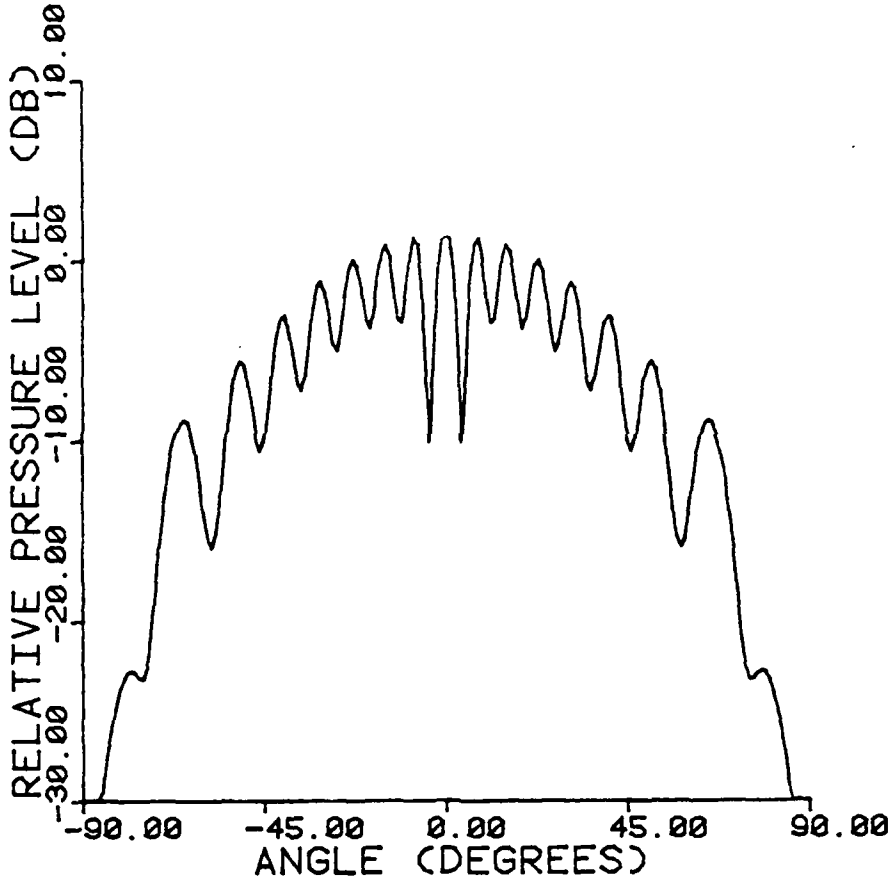

Figure 13. Calculated directivity pattern at 40 kHz for an LC-10 hydrophone 0.375" from a grating of 15 slits and on the axis of symmetry of the grating.

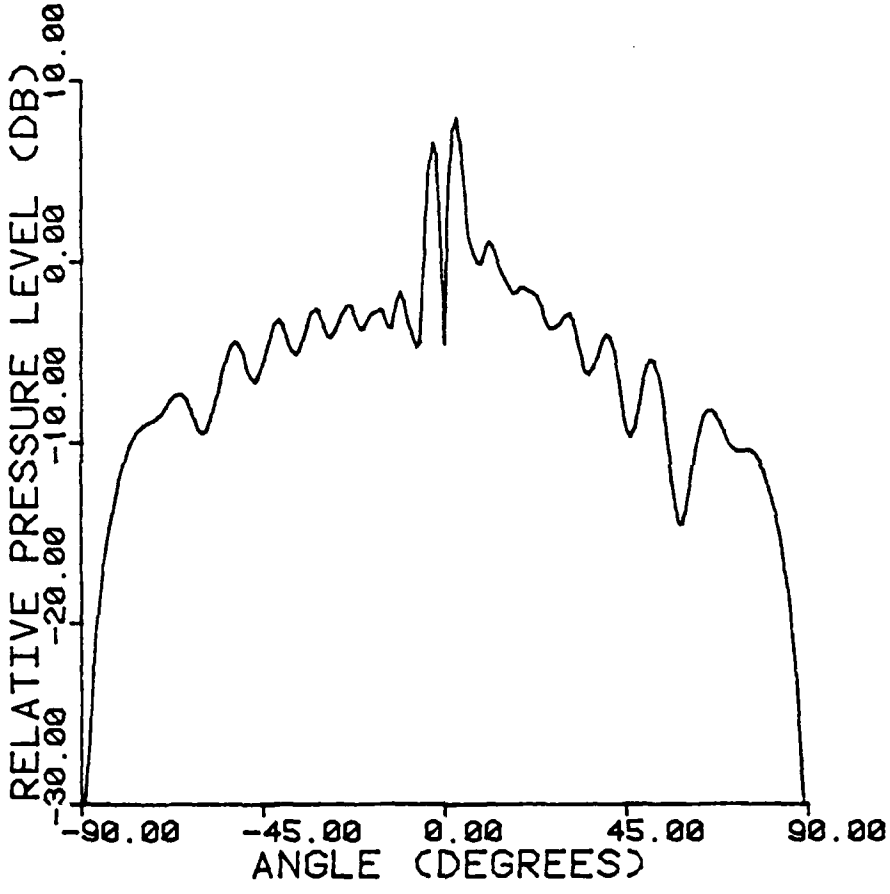

Figure 14. Calculated directivity pattern at 40 kHz for an LC-10 hydrophone 0.375" from a grating of 15 slits and 0.375" off the axis of symmetry.

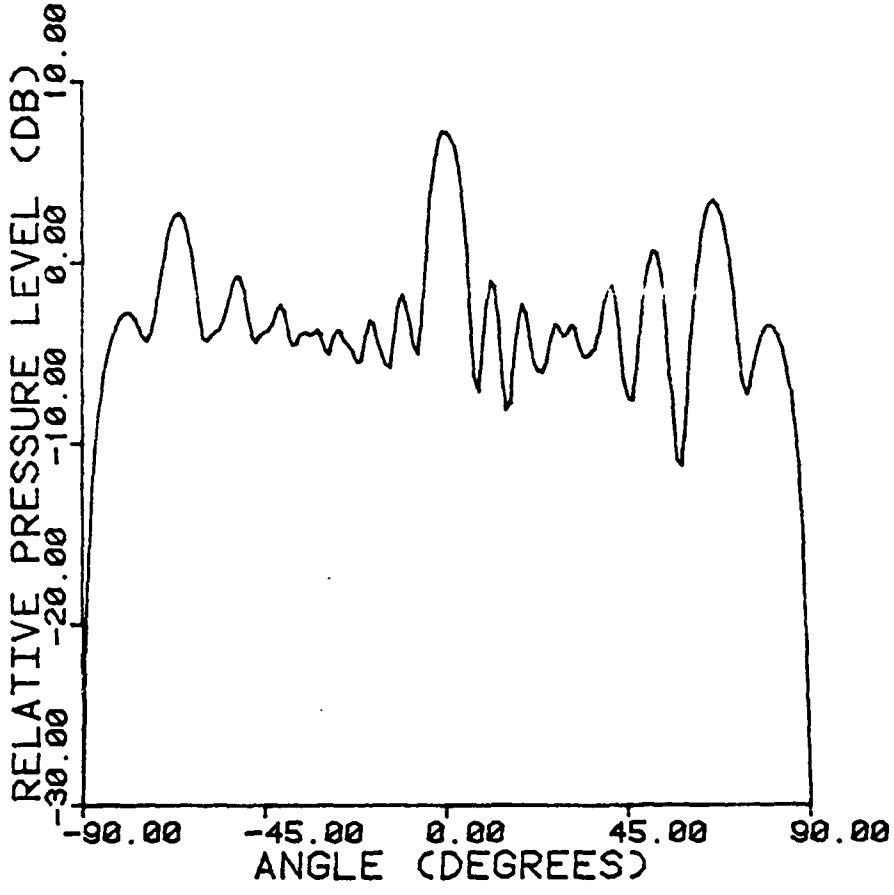

Figure 15. Calculated directivity pattern at 40 kHz for an LC-10 hydrophone 0.375" from a grating of 15 slits and 0.75" off the axis of symmetry (directly behind a styrofoam strip).

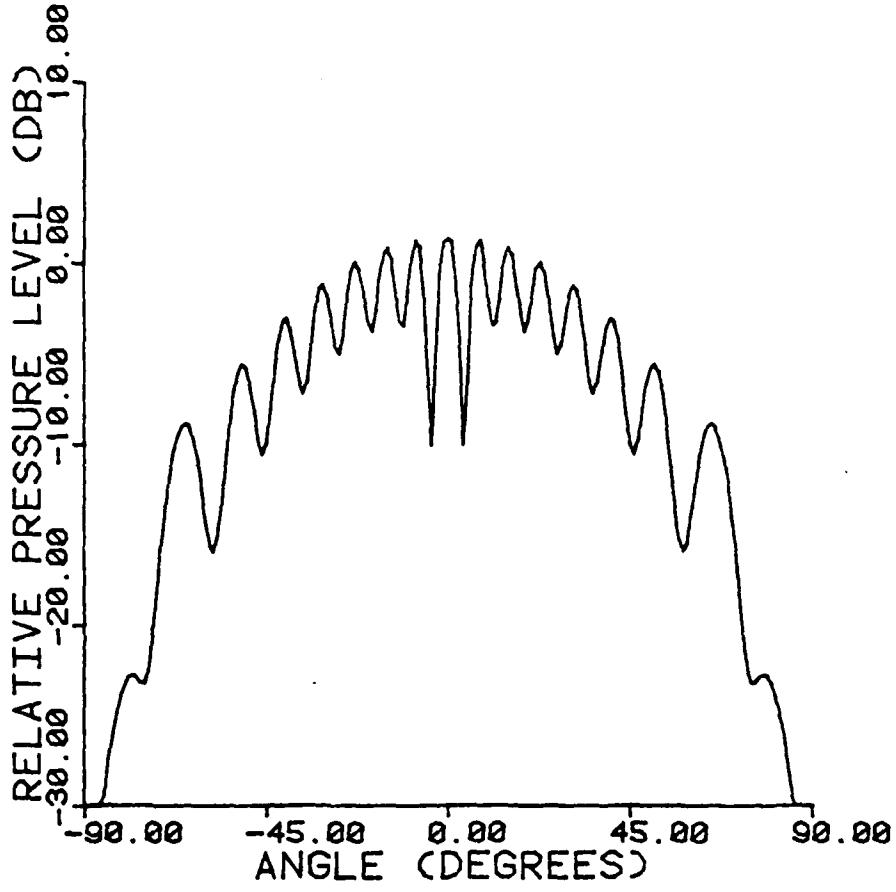

Figure 16. Calculated directivity pattern for a grating of 15 slits at 40 kHz. The LC-10 hydrophone is 0.375" from the grating and on the axis of symmetry of the grating.

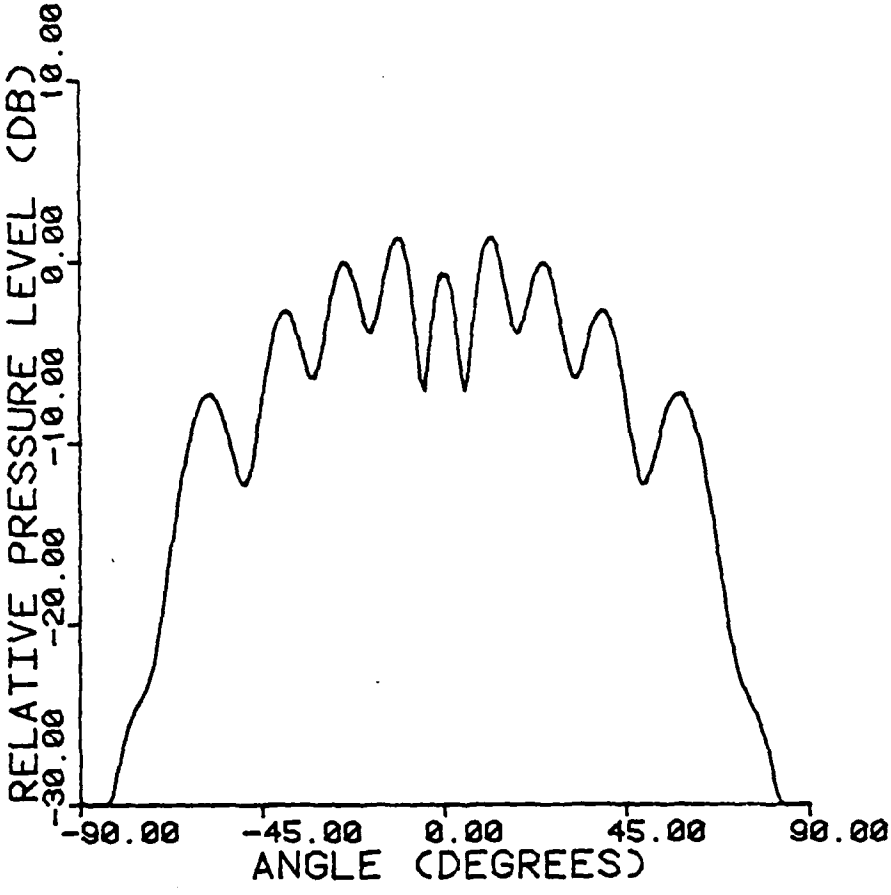

Figure 17. Calculated directivity pattern for a grating of 9 slits at 40 kHz. The LC-10 hydrophone is 0.375" from grating and on the axis of symmetry of the grating.

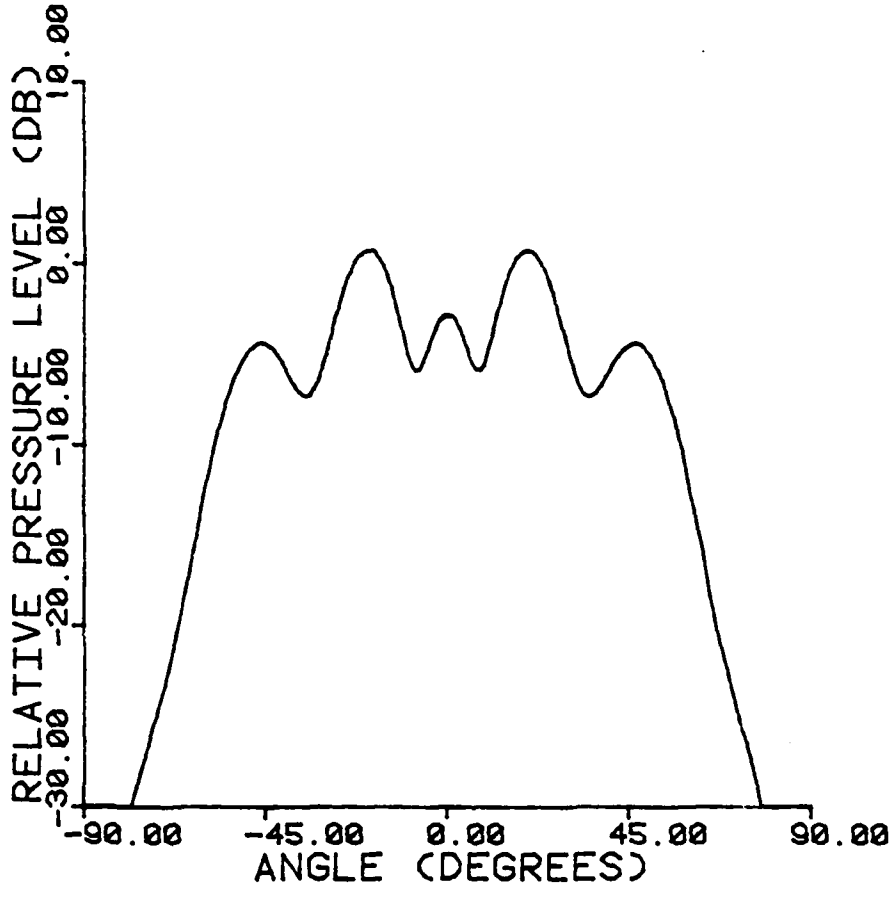

Figure 18. Calculated directivity pattern for a grating of 5 slits at 40 kHz. The LC-10 hydrophone is 0.375" from the grating and on the axis of symmetry of the grating.

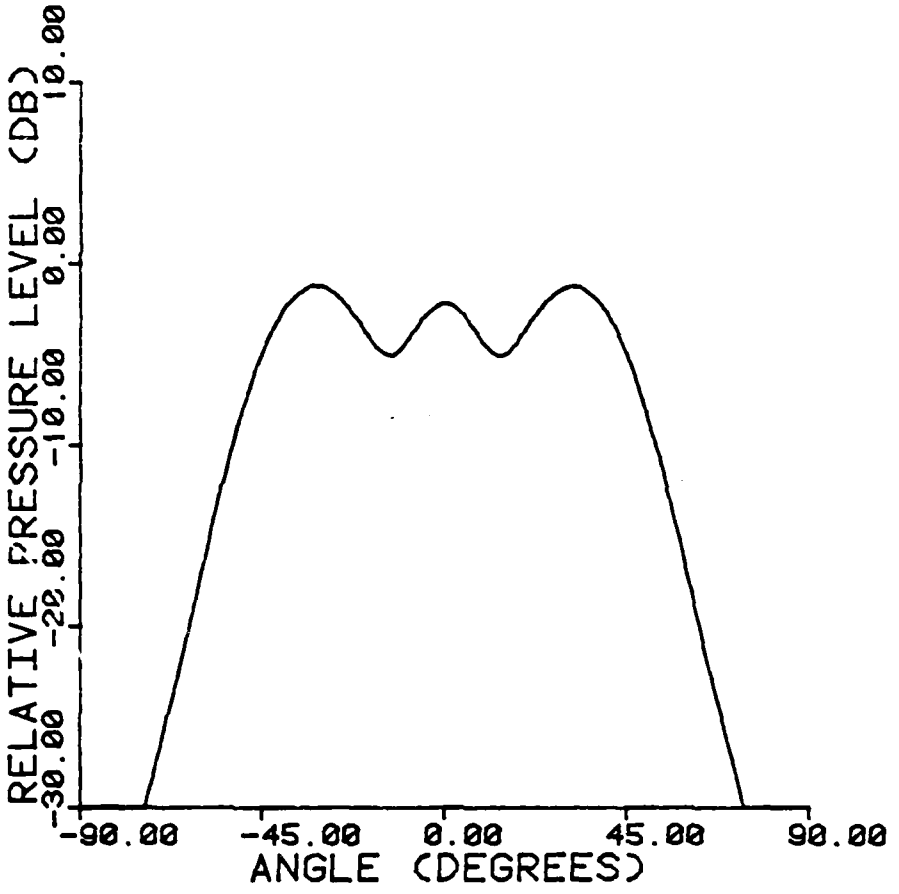

Figure 19. Calculated directivity pattern for a grating of 3 slits at 40 kHz. The LC-10 hydrophone is 0.375" from the grating and on the axis of symmetry of the grating.

2. α decreases in magnitude to approximately zero as the hydrophone moves from behind a slit to behind a strip
3. α remains constant as the number of slits changes provided the number of slits does not become too small.

To justify the above assertions, a geometrical analysis was performed similar to the analysis used to produce the solid curve in Figure 5. A computer program was written to calculate high frequency directivity patterns for a specified grating structure and hydrophone position and smooth the resulting patterns into a roughly parabolic shape. While the values of α predicted by this program were generally higher in magnitude than those obtained from experiment, indicating that more energy is transmitted through the grating at high angles by various scattering mechanisms than can be accounted for by a consideration of geometrical shadowing, the results do support the above assertions.

3.3 Incident Cylindrical Waves

3.3.1 Expression for the transmitted sound field. Consider a finite number of slits of width a and infinite length in an opaque screen of infinite extent placed symmetrically in the $z = 0$ plane of a rectangular coordinate system. Let the edges of the slits be parallel to the y axis and separated by a width b of screen, as in Figure 20.

For a line source through the point $(x_o, 0, z_o < 0)$ and parallel to the y axis, the emitted sound pressure can be written as [8]

$$p = A[J_o(kr) + iN_o(kr)],$$

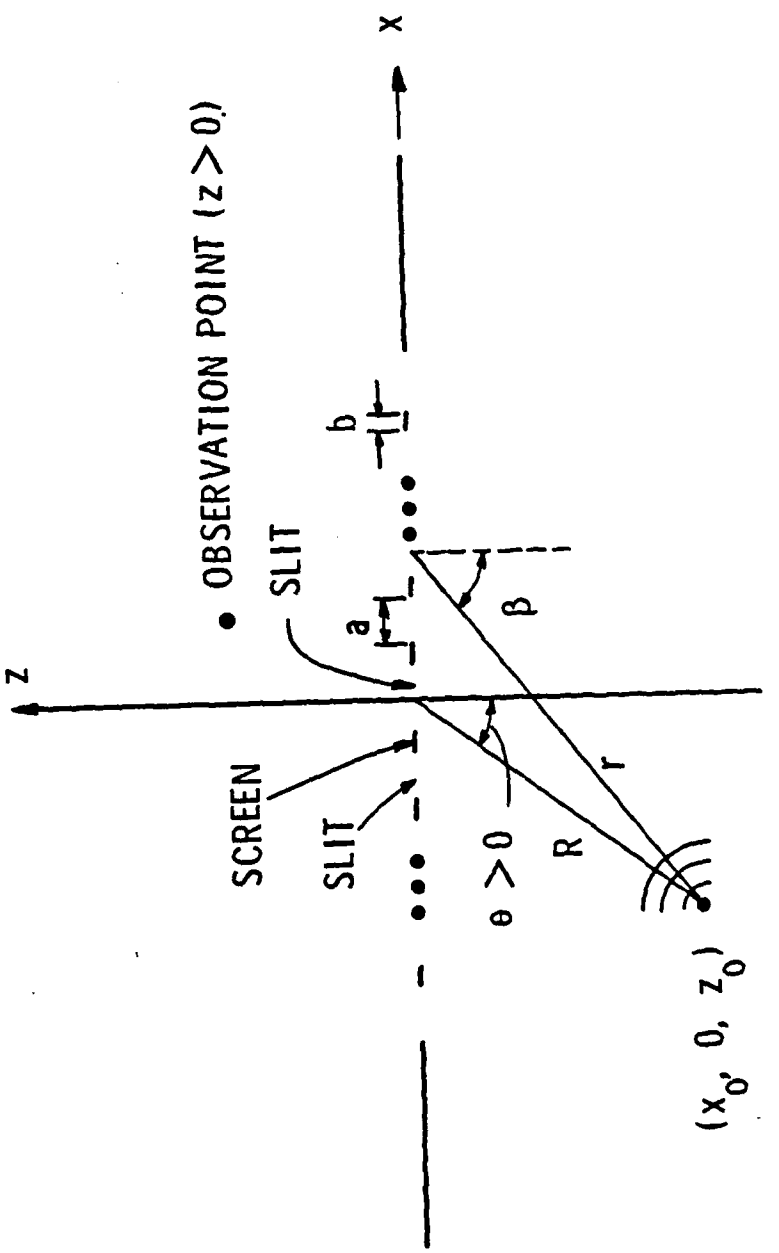

Figure 20. Reference geometry for incident cylindrical waves.

where $r = \sqrt{(x-x_o)^2 + (z-z_o)^2}$, A is a normalization constant, and J_o and N_o are the Bessel functions of the first and second kind, respectively, of order zero. Then the particle velocity in the radial direction is

$$u_r = \frac{1}{i\omega\rho} \frac{dp}{dr} = - \frac{Ak}{i\omega\rho} [J_1(kr) + i\, N_1(kr)]$$

which, on substitution for r , becomes

$$u_r(x,z) = - \frac{Ak}{i\omega\rho} [J_1(k \sqrt{(x-x_o)^2 + (z-z_o)^2}) + iN_1(k \sqrt{(x-x_o)^2 + (z-z_o)^2})],$$

where J_1 and N_1 are the Bessel functions of the first and second kind, respectively, of order one. Hence, we assume the component of the particle velocity in the z direction evaluated in the z = 0 plane becomes (Figure 20)

$$u_z(x) = u_r(x,0)f(x)\cos\beta = \frac{|z_o|}{r} u_r(x,0)f(x),$$

where f(x) is a function having the value one for all points (x,y,0) in the slits and zero for all other points in the plane of the grating and $r = \sqrt{(x-x_o)^2 + z_o^2}$.

By a procedure similar to that used to derive Equation (3.2.1.2) it can be shown that

$$p(x,z) = -i\omega\rho\, F_1^{-1} [u_z(k_x)\, G_N(k_x,0,z)], \qquad (3.3.1.1)$$

where $G_N(k_x,k_y,z)$ is given by Equation (2.2.4) and

$$u_z(k_x) = F_1[u_z(x)]. \qquad (3.3.1.2)$$

Equation (3.3.1.2) must be evaluated numerically as it involves integrals of the form

$$\int_{\alpha}^{\beta} (x^2 + \gamma^2)^{-\frac{1}{2}} Z_1(k\sqrt{x^2+\gamma^2})\, e^{-ik_x x}\, dx,$$

where Z_1 equals J_1 or N_1 and α, β, and γ are constants.

3.3.2 Calculated Results. Directivity patterns are computed for the case of three slits of width 1.125 inches separated by 0.375 inches of screen for a hydrophone located at the point (0,0,0.375)(i.e., on the z axis and 0.375 inches above the z = 0 plane) by evaluating Equation (3.3.1.1) for fixed R (Figure 20), where R equals the distance of the line source from the center of the grating, while letting θ (Figure 20) range from -90° to +90° and then adding a parabola of the form $\alpha\theta^2$ to the resulting directivity patterns since we wish to consider a grating composed of strips extended 0.375 inches in the direction normal to the grating. α is assumed to take on the values given in Figure 9. This assumption can be expected to hold for a line source at least a few wavelengths from the grating.

The results of this investigation are contained in Figures 22, 23, and 24 for ν = 40 kHz and R = 3 inches, 5 inches, and 10 inches, respectively, in Figures 26, 27, and 28 for ν = 33 kHz and R = 3 inches, 5 inches, and 10 inches, respectively, and in Figures 30, 31, and 32 for ν = 25 kHz and R = 3 inches, 5 inches, and 10 inches, respectively. The value of α used in Figure 30 ($\alpha = -10\times10^{-4}$) may be questionable as

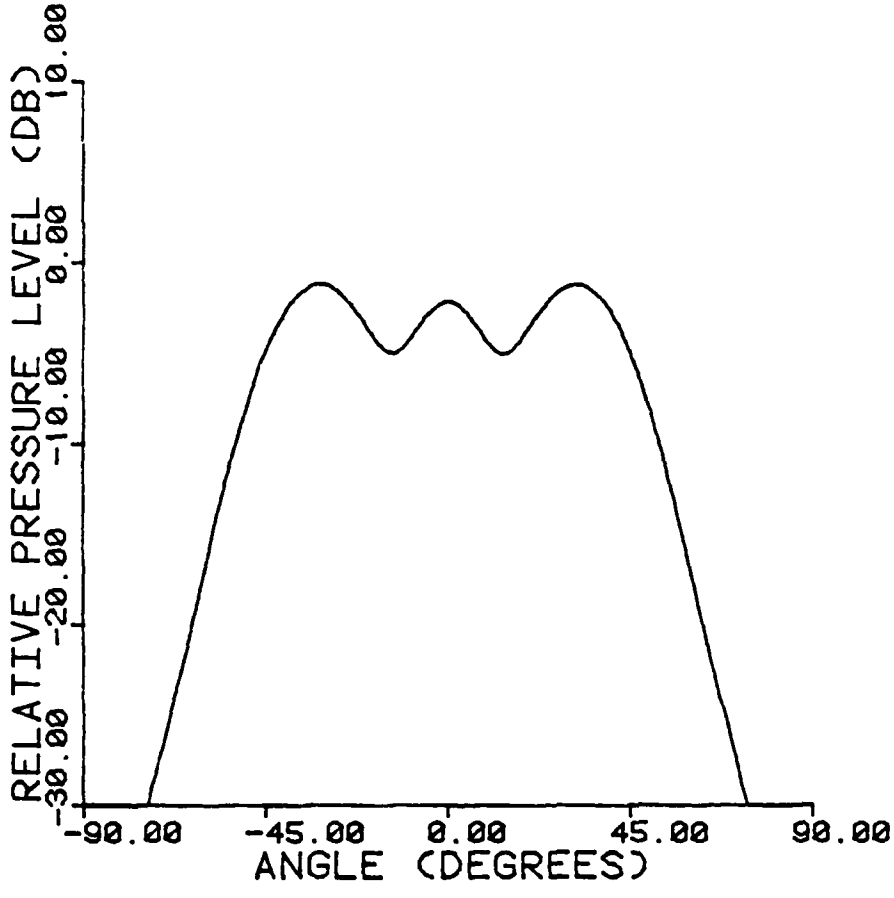

Figure 21. Calculated directivity pattern (grating of 3 straight slits) for 40 kHz incident plane waves. The LC-10 hydrophone is 0.375" behind the grating and on the axis of symmetry of the grating.

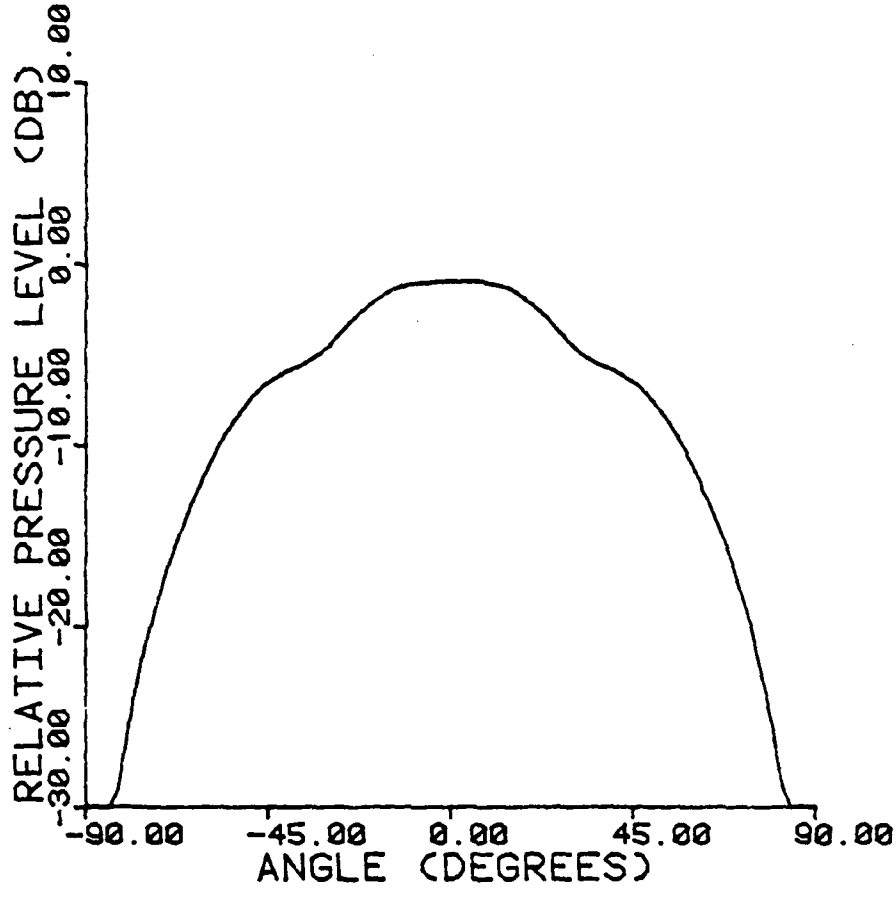

Figure 22. Calculated directivity pattern (grating of 3 straight slits) for 40 kHz waves emitted by a line source 3" from the center of the grating.

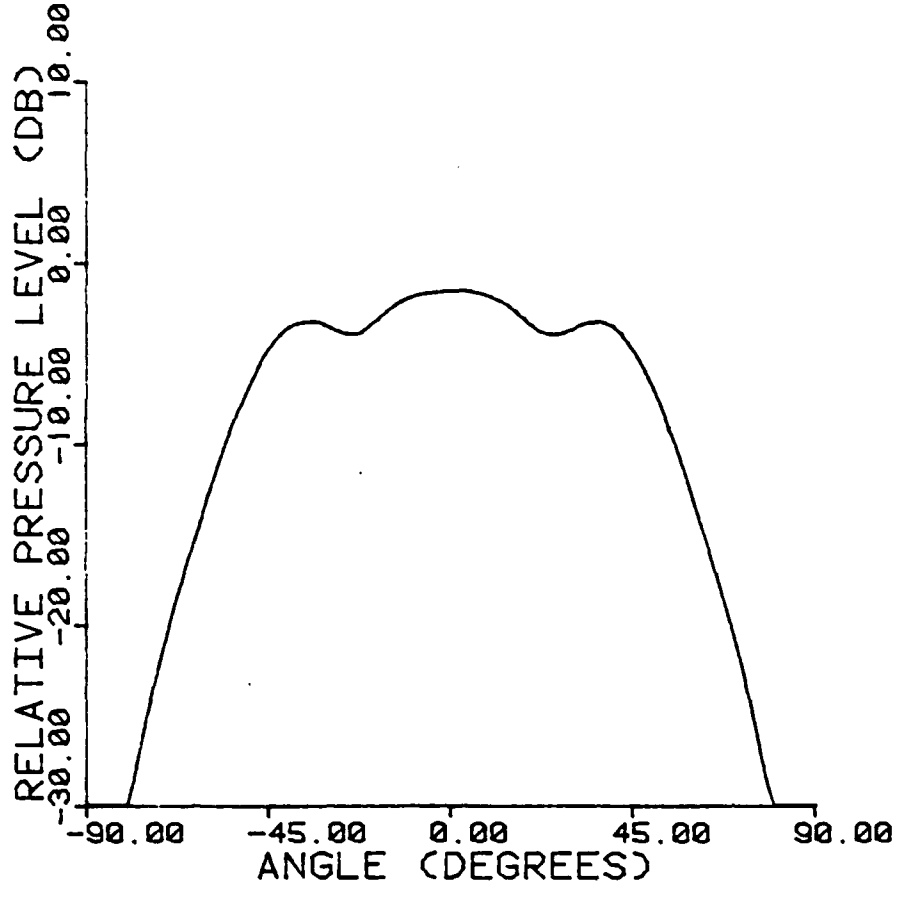

Figure 23. Calculated directivity pattern (grating of 3 straight slits) for 40 kHz waves emitted by a line source 5" from the center of the grating.

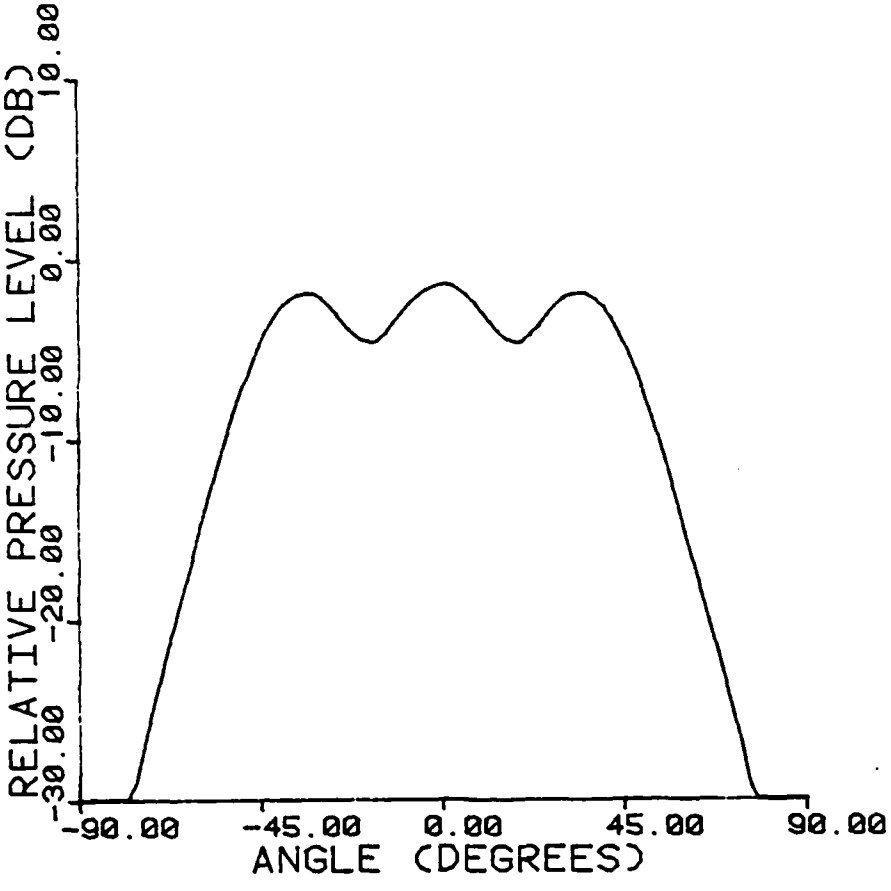

Figure 24. Calculated directivity pattern (grating of 3 straight slits) for 40 kHz waves emitted by a line source 10" from the center of the grating (cf. Figure 21).

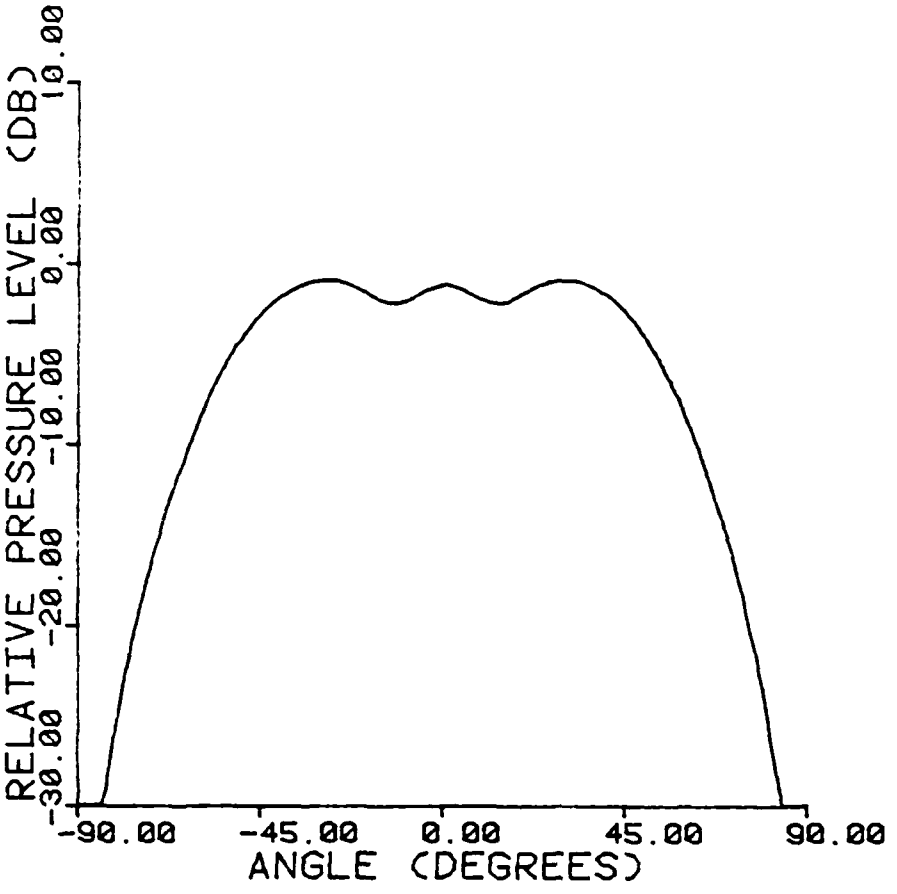

Figure 25. Calculated directivity pattern (grating of 3 straight slits) for 33 kHz incident plane waves.

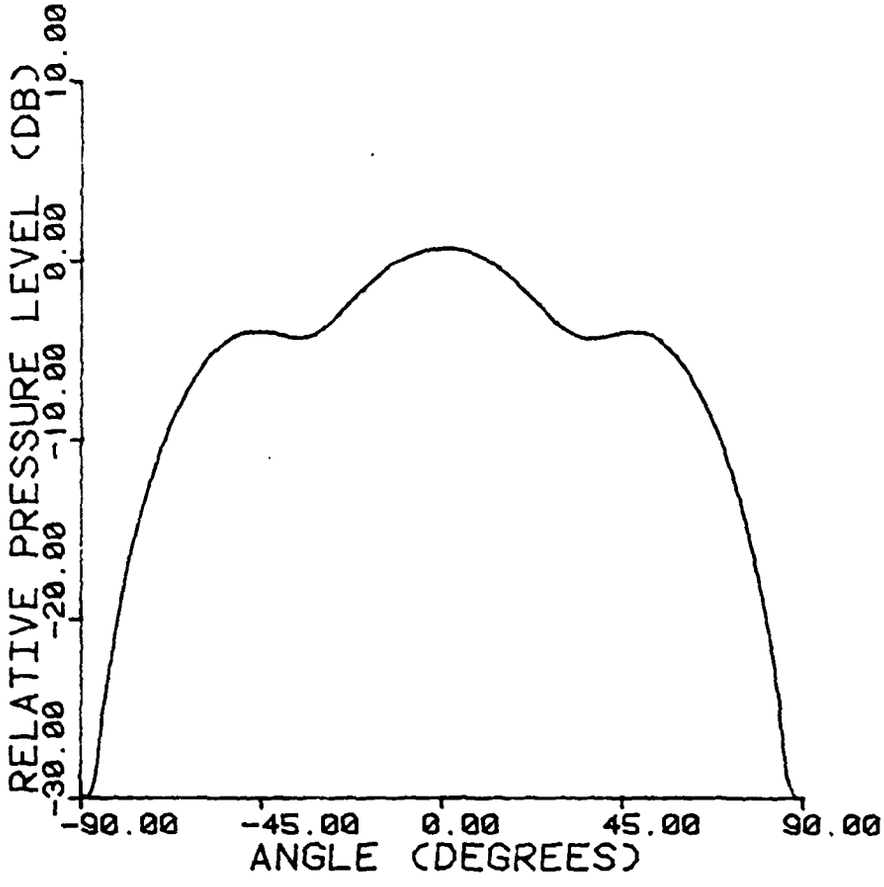

Figure 26. Calculated directivity pattern (grating of 3 straight slits) for 33 kHz waves emitted by a line source 3" from the center of the grating.

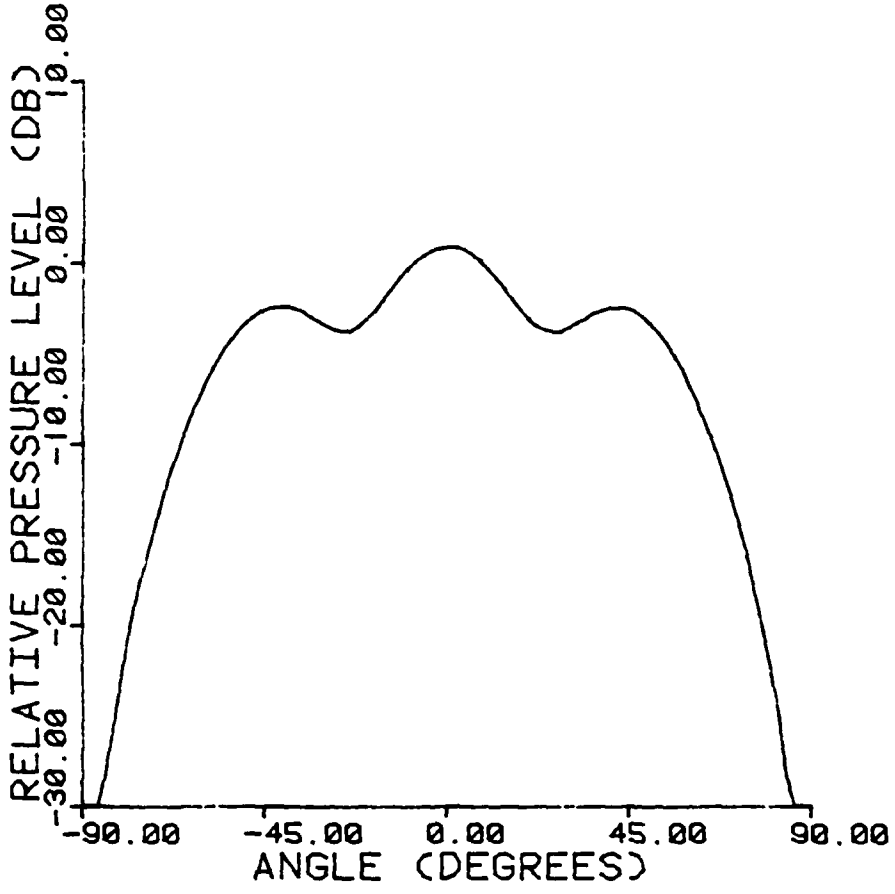

Figure 27. Calculated directivity pattern (grating of 3 straight slits) for 33 kHz waves emitted by a line source 5" from the center of the grating.

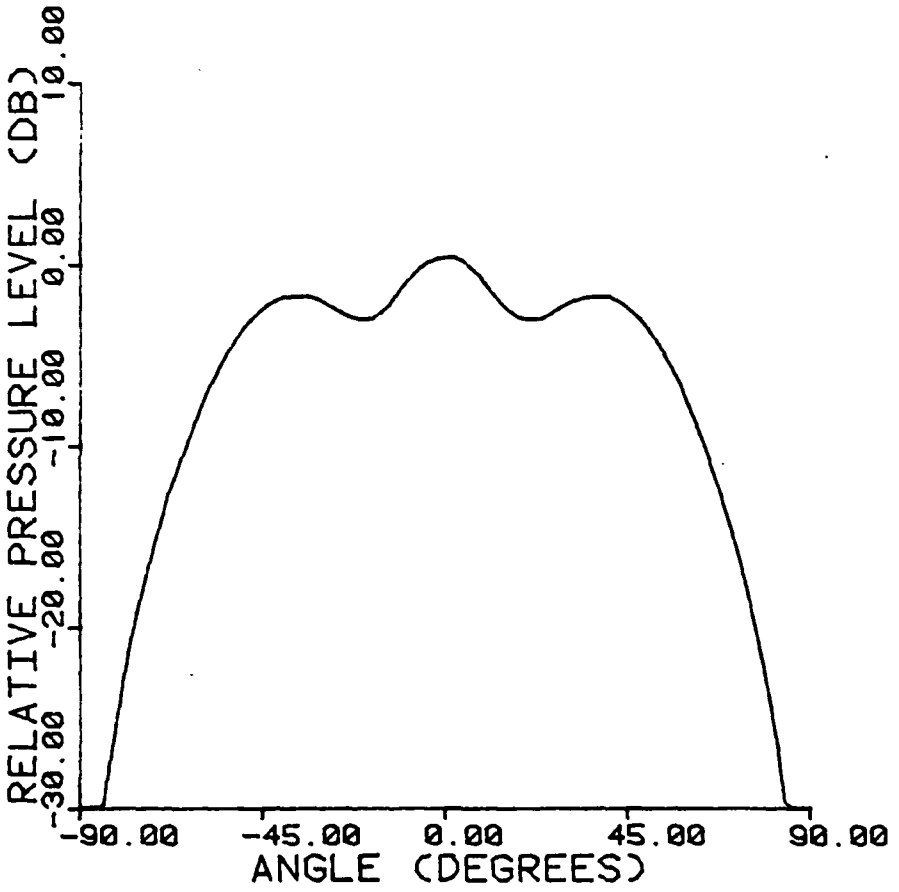

Figure 28. Calculated directivity pattern (grating of 3 straight slits) for 33 kHz waves emitted by a line source 10" from the center of the grating (cf. Figure 25).

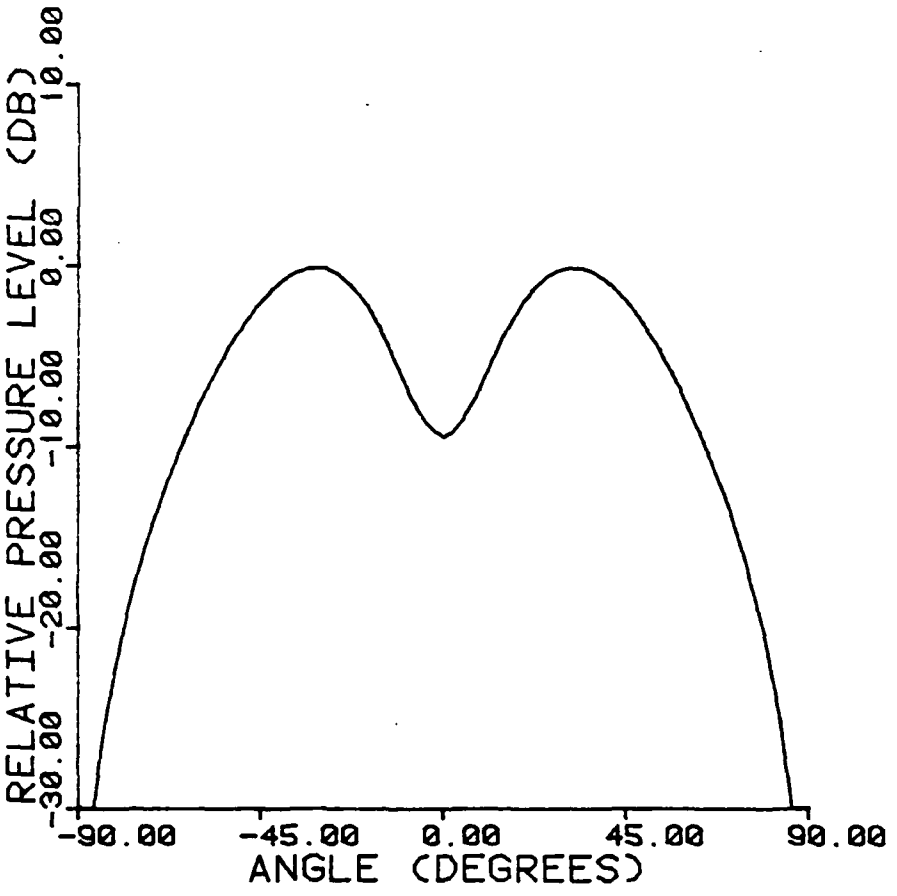

Figure 29. Calculated directivity pattern (grating of 3 straight slits) for 25 kHz incident plane waves.

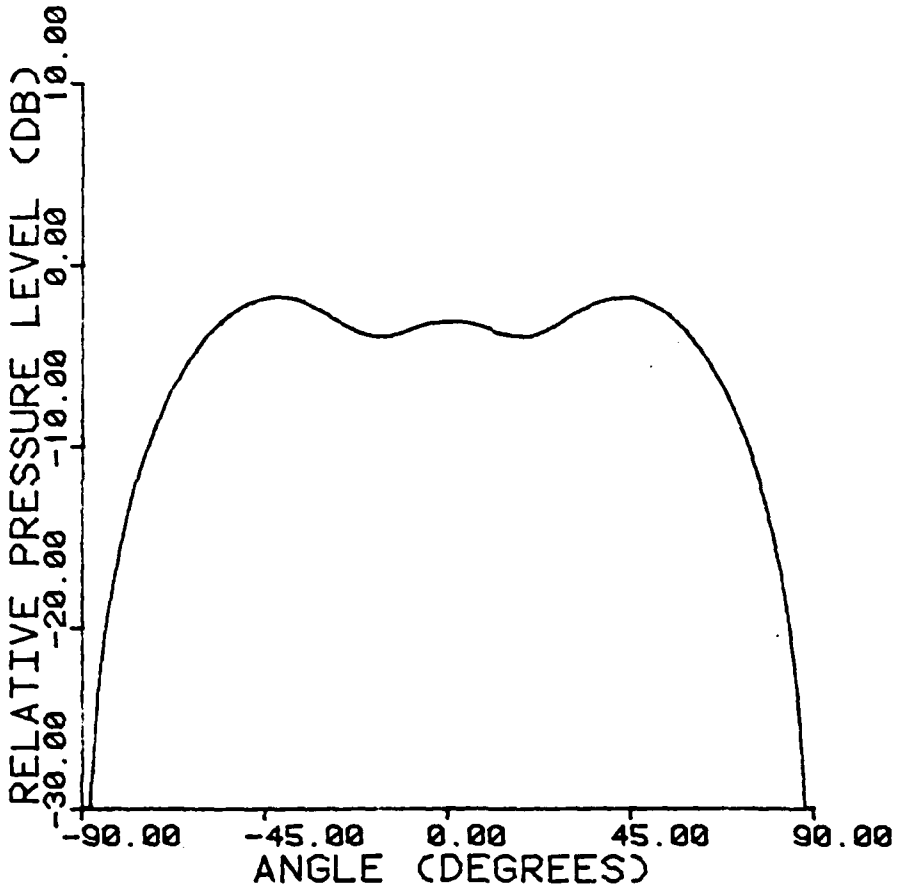

Figure 30. Calculated directivity pattern (grating of 3 straight slits) for 25 kHz waves emitted by a line source 3" from the center of the grating.

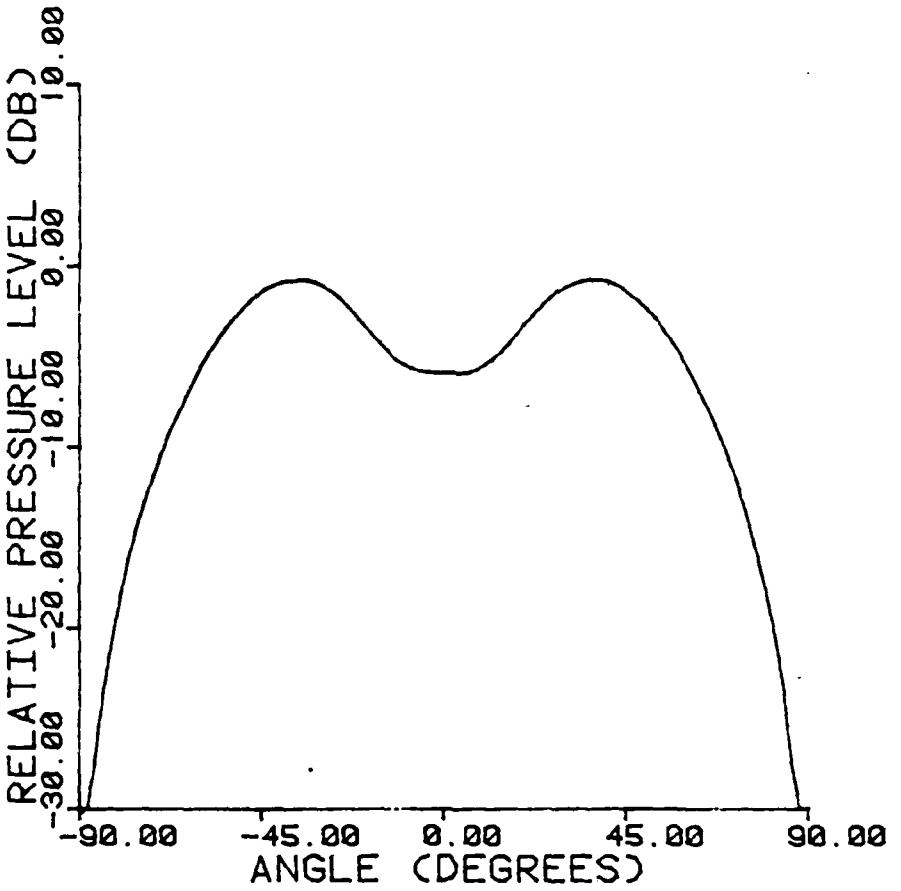

Figure 31. Calculated directivity pattern (grating of 3 straight slits) for 25 kHz waves emitted by a line source 5" from the center of the grating.

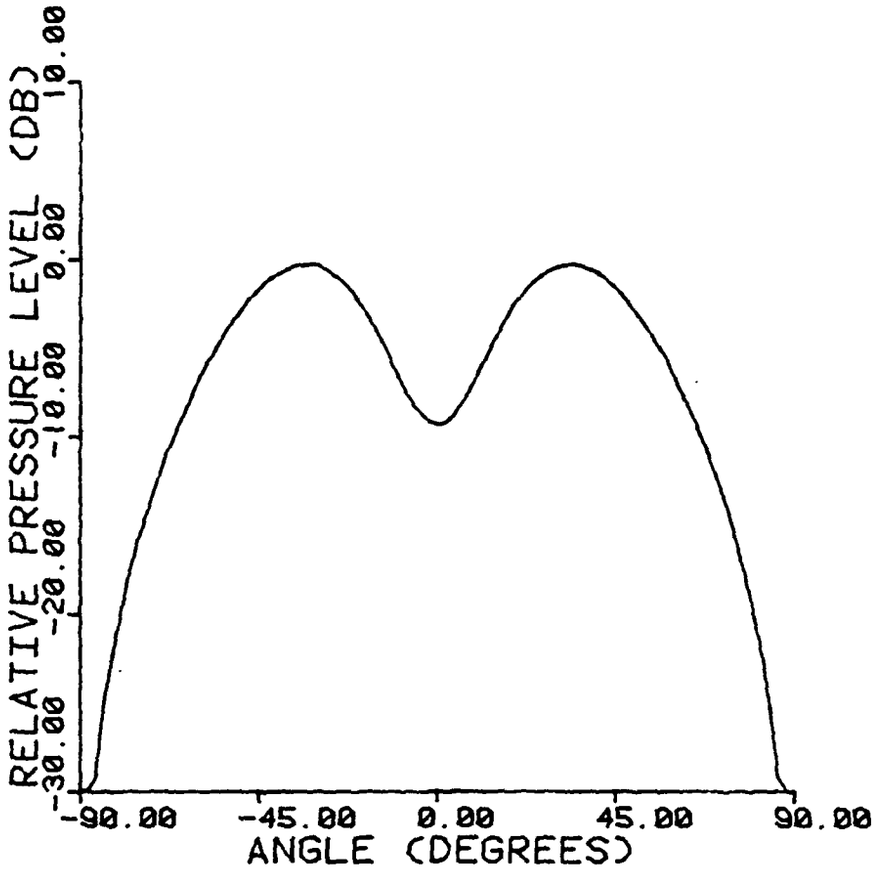

Figure 32. Calculated directivity pattern (grating of 3 straight slits) for 25 kHz waves emitted by a line source 10" from the center of the grating (cf. Figure 29).

the source is about one wavelength from the center of the grating. Figures 21, 25, and 29 for incident plane waves at ν = 40 kHz, 33 kHz, and 25 kHz are provided for purposes of comparison. All of the data in the above mentioned figures have been normalized with respect to the pressure measured by the hydrophone with no screen present between the source and receiver. Therefore, the maximum pressure attained in each directivity pattern is, as expected, fairly constant from one figure to the next. If, instead, a constant normalization is chosen, then one observes the expected $s^{-\frac{1}{2}}$ dependence of the magnitude of the pressure behind the grating on the distance s from the receiver to the source.

Two more observations worthy of note can be made here. As the distance R of the source from the center of the grating increases, the directivity pattern converges to the directivity pattern calculated for incident plane waves. Furthermore, for a line source close to the grating, the directivity pattern is broadened and smooth as compared with the pattern calculated for incident plane waves, although the property of discrimination against grazing incidence sound waves that seems to be characteristic of any grating extended in the direction normal to the grating is not unduly affected.

CHAPTER IV

GRATING OF CONCENTRIC RINGS

4.1 Introduction

In this chapter, we consider the nearfield of a grating consisting of concentric rings in an infinitely extended opaque screen. To avoid having to evaluate Equation (2.2.3), we restrict discussion to the case where the point of observation lies on the axis through the center of the grating and perpendicular to the screen. In the following discussion, we assume, of course, that the particle velocity in the circular slits is the same as if no grating were present and zero everywhere else in the plane of the grating.

4.2 Expression for the Transmitted Sound Field

Consider a grating consisting of concentric rings in an infinite, opaque screen placed symmetrically in the $z = 0$ plane and insonified by a plane wave having a wave vector $\bar{k}$ perpendicular to the y axis and making an angle θ with respect to the z axis. For r equal to the distance from the origin in the $z = 0$ plane and ϕ equal to the polar angle in the $z = 0$ plane, we assume that the z component of the particle velocity in the plane of the grating is

$$u_z(r,\phi) = f(r)u_o \cos\theta \exp(ikr\sin\theta\cos\phi) ,$$

where u_o is the amplitude of the particle velocity of the incident plane wave (incident from the negative z direction), $f(r)$ is a function having the value one for a point (r,ϕ) in the circular

slits and zero everywhere else in the z = 0 plane, and $k = |\bar{k}| = \frac{2\pi}{\lambda}$. Hence, the pressure at a point on the z axis having coordinates (0,0,z>0) can be written as [6]

$$p(z) = \frac{-i\rho ck}{2\pi} u_o \cos\theta \int_0^{\infty} \int_0^{2\pi} f(r) \exp(ikr\sin\theta\cos\phi) [\exp(ik\sqrt{z^2+r^2})/\sqrt{z^2+r^2}] r d\phi dr$$

which can be simplified to

$$p(z) = -i\rho cku_o \cos\theta \int_0^{\infty} f(r) J_o(kr\sin\theta) [\exp(ik\sqrt{z^2+r^2})/\sqrt{z^2+r^2}] r dr. \quad (4.2.1)$$

The results of a numerical evaluation of above integral are presented in the following section.

4.3 Calculated Results

In Figure 33, the geometrical configuration of the grating to be considered in this section and a numbering scheme to be used in discussing subsequent results are described. Because we are considering a grating with some extent (0.375 inches) in the direction normal to the grating, it is necessary to add a parabola of the form $\alpha\theta^2$ to the directivity patterns obtained from the Simpson's rule evaluation of Equation (4.2.1). By a consideration of Figure 2 and 33, it becomes apparent that α, for 40 kHz incident plane waves, can be assumed to be -30×10^{-4}.

The effects on the directivity pattern of moving the hydrophone away from the grating are considered in Figures 34, 35, and 36 for 40 kHz plane waves incident on a grating having eight circular spaces (L=8). α is assumed to remain constant for excursions of the hydrophone from the grating less than 1.5 inches for the

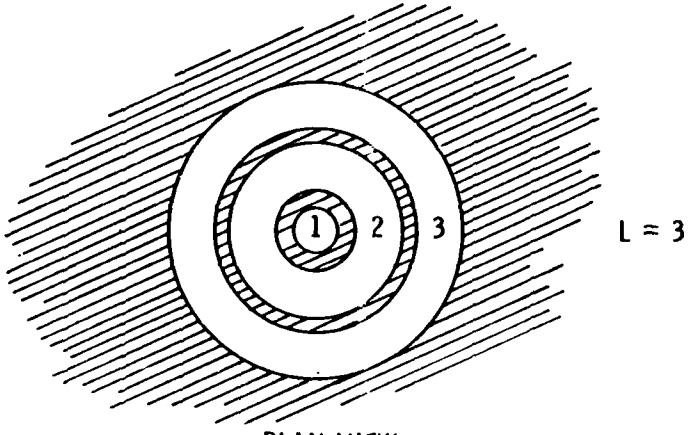

PLAN VIEW

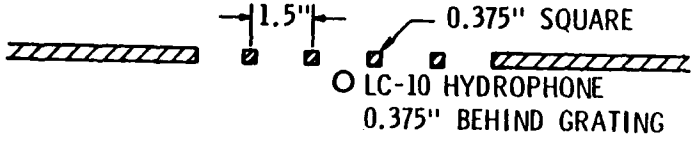

SIDE VIEW

Figure 33. Geometrical configuration for diffraction through a grating of concentric rings (cf. Figure 2) for the case of L=3 (3 circular spaces). The shaded regions correspond to screen.

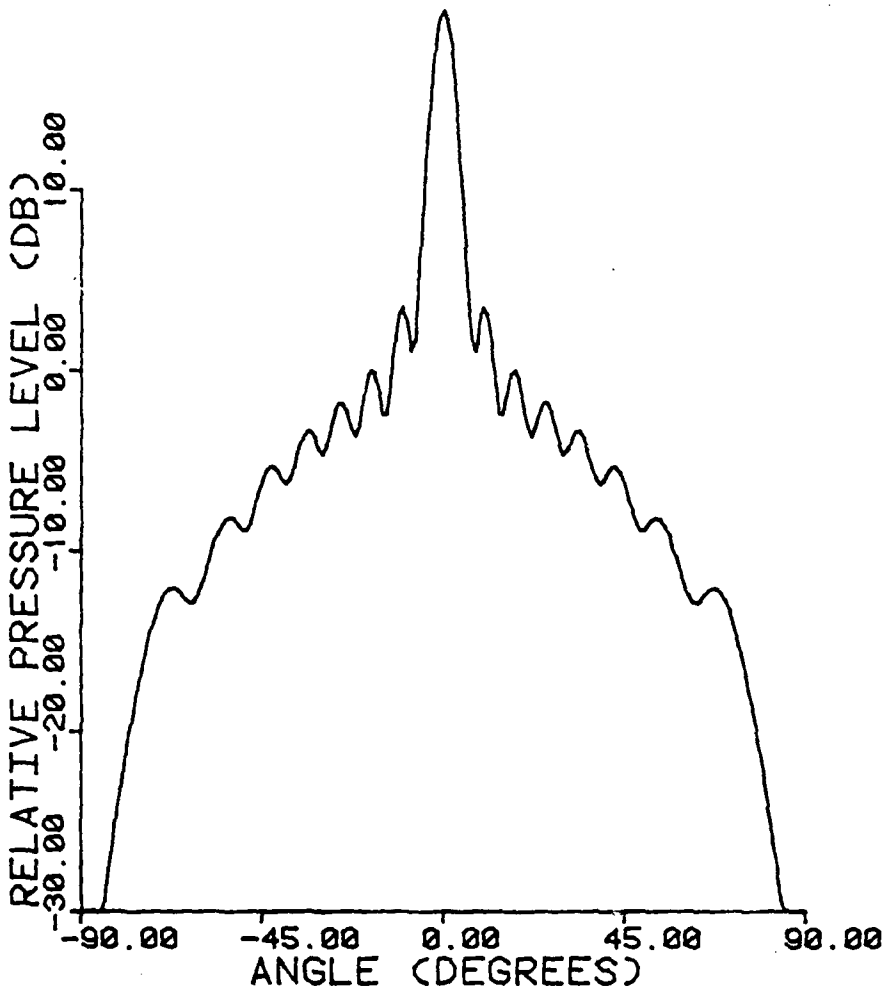

Figure 34. Calculated directivity pattern (concentric rings, L=8) for 40 kHz plane waves. The LC-10 hydrophone is on the axis of symmetry and 0.1" from the grating.

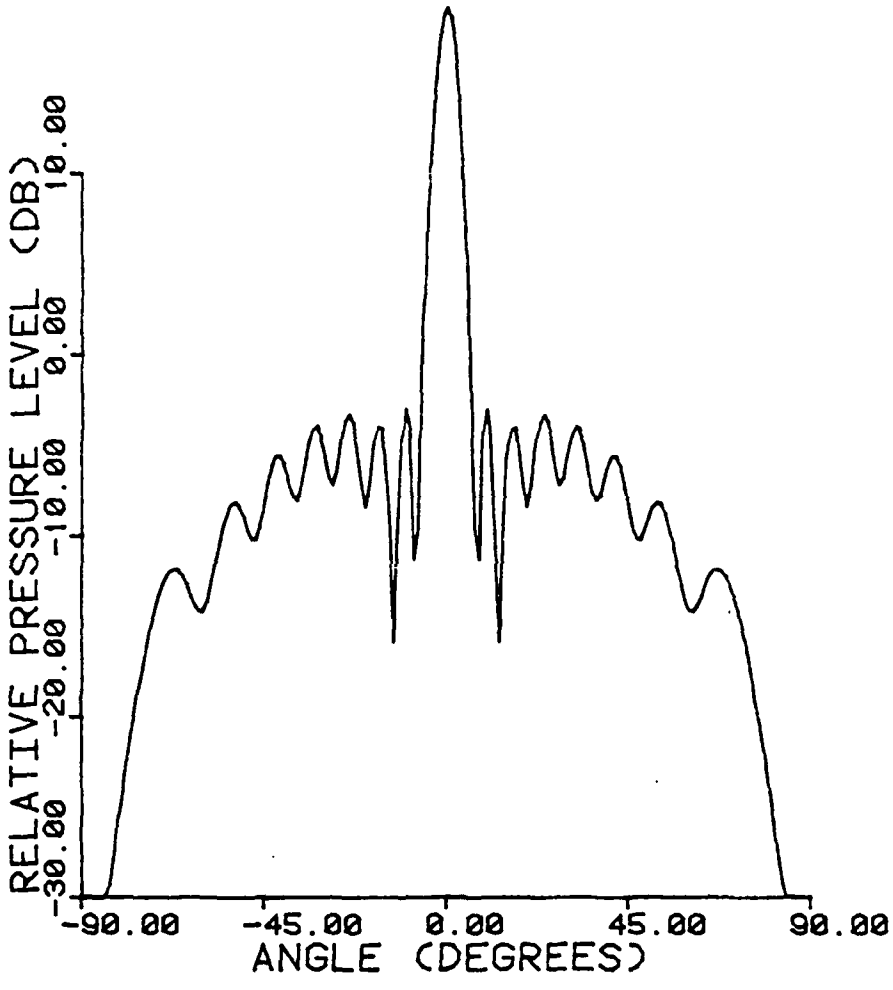

Figure 35. Calculated directivity pattern (concentric rings, L=8) for 40 kHz plane waves. The LC-10 hydrophone is on the axis of symmetry and 0.4" from the grating.

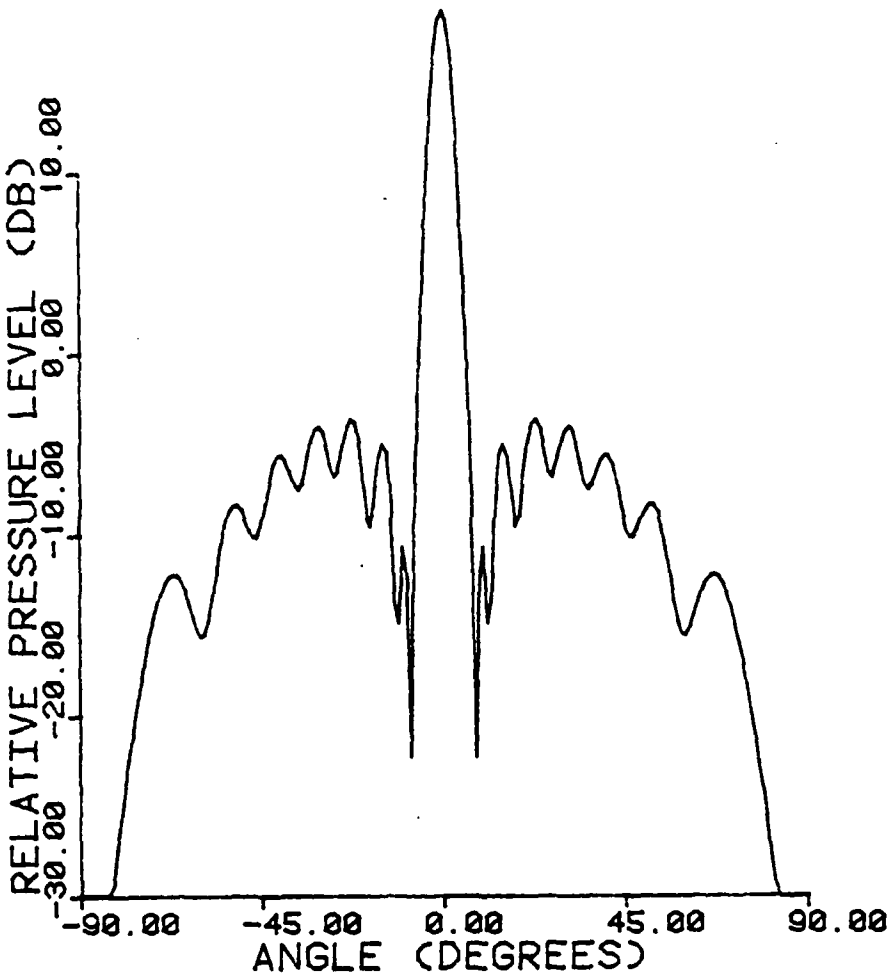

Figure 36. Calculated directivity pattern (concentric rings, L=8) for 40 kHz plane waves. The LC-10 hydrophone is on the axis of symmetry and 0.7" from the grating.

geometry considered here. Clearly, as the distance of the hydrophone from the grating increases, the central spike, characteristic of directivity patterns at this frequency, remains relatively unaffected while the response at higher angles decreases.

As can be seen from Figures 37, 38, 39, and 40, as the number of circular spaces in the grating decreases, the central spike decreases in height and broadens. α is assumed to remain relatively unaffected as the number of circular spaces changes.

Finally, the frequency response for normal incidence plane waves is presented in Figure 41 for a hydrophone on the axis of symmetry of a grating having eight circular slits and 0.375 inches from the grating. Note the peaks in the response at approximately full wavelength spacing (40 kHz), $\frac{3}{4}$ wavelengths spacing (30 kHz), $\frac{5}{8}$ wavelengths spacing (25 kHz), half wavelength spacing (20 kHz), and $\frac{3}{8}$ wavelengths spacing (15 kHz). The grating appears to behave as a condensing lens particularly well at 40 kHz.

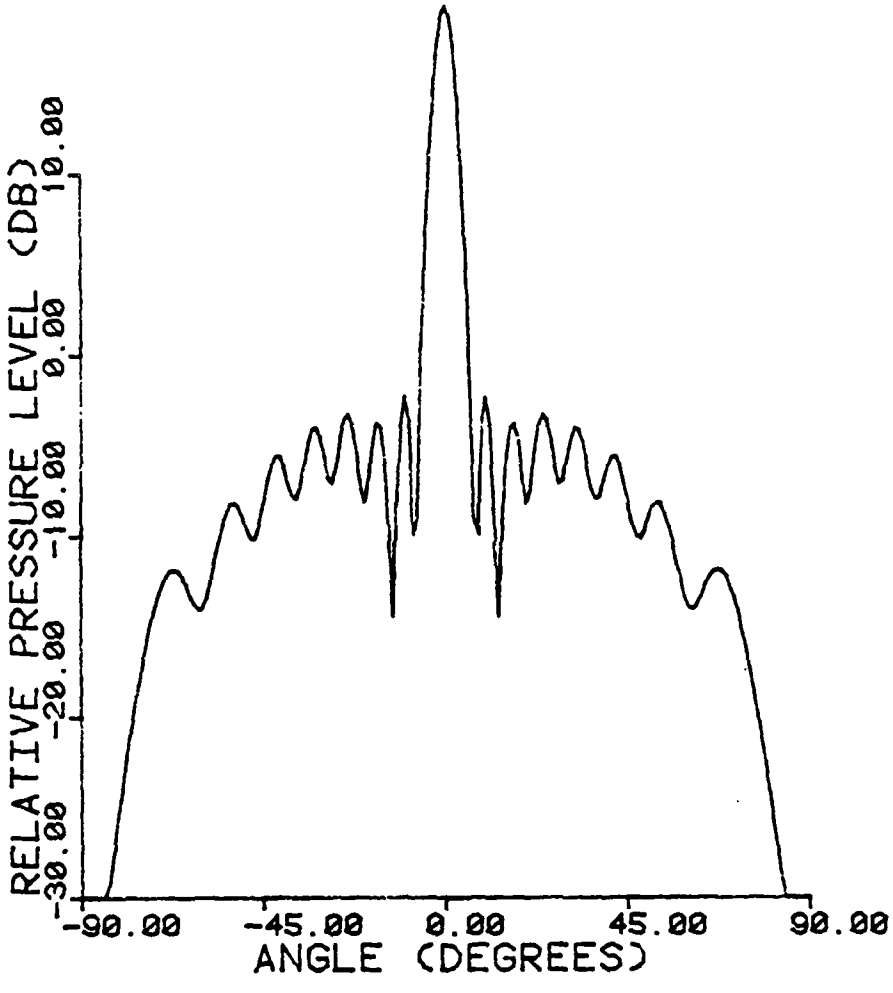

Figure 37. Calculated directivity pattern (concentric rings, L=8) for 40 kHz plane waves. The LC-10 hydrophone is on the axis of symmetry and 0.375" from the grating.

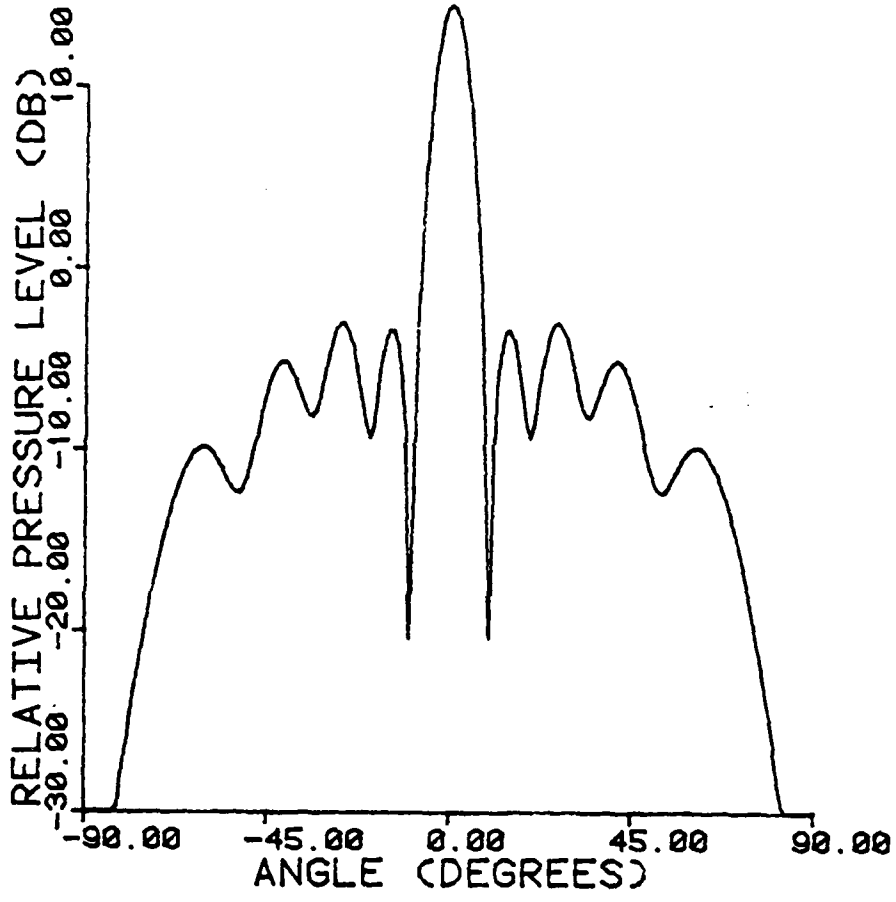

Figure 38. Calculated directivity pattern (concentric rings, L=5) for 40 kHz plane waves. The LC-10 hydrophone is on the axis of symmetry and 0.375" from the grating.

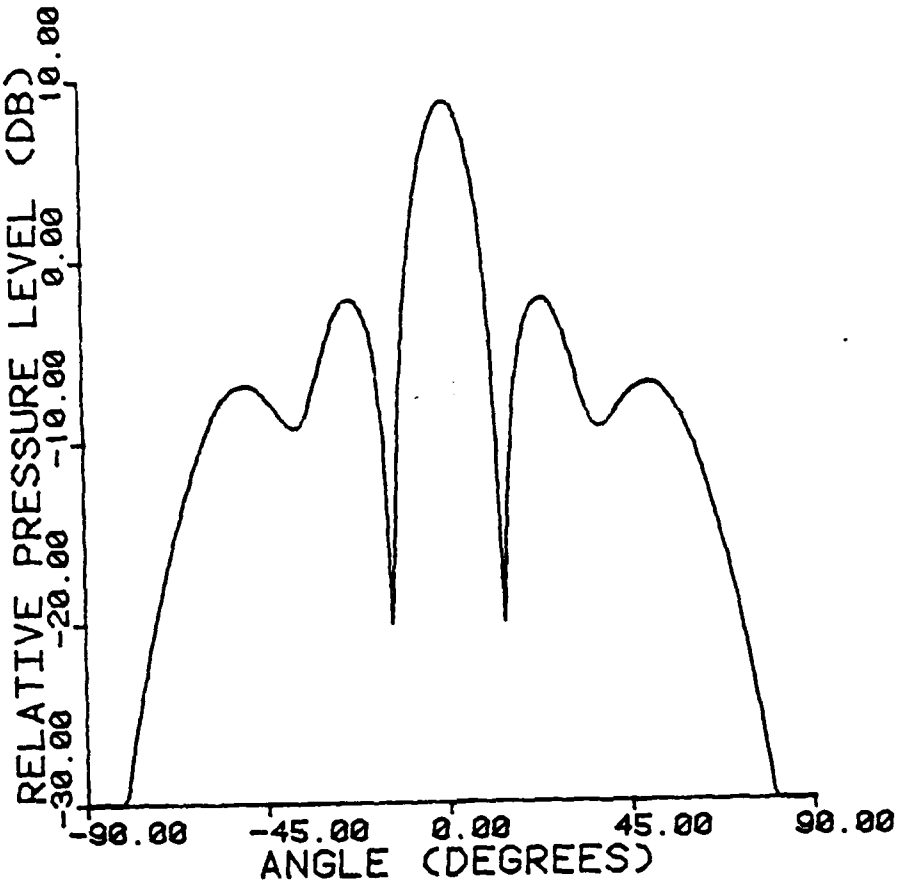

Figure 39. Calculated directivity pattern (concentric rings, L=3) for 40 kHz plane waves. The LC-10 hydrophone is on the axis of symmetry and 0.375" from the grating.

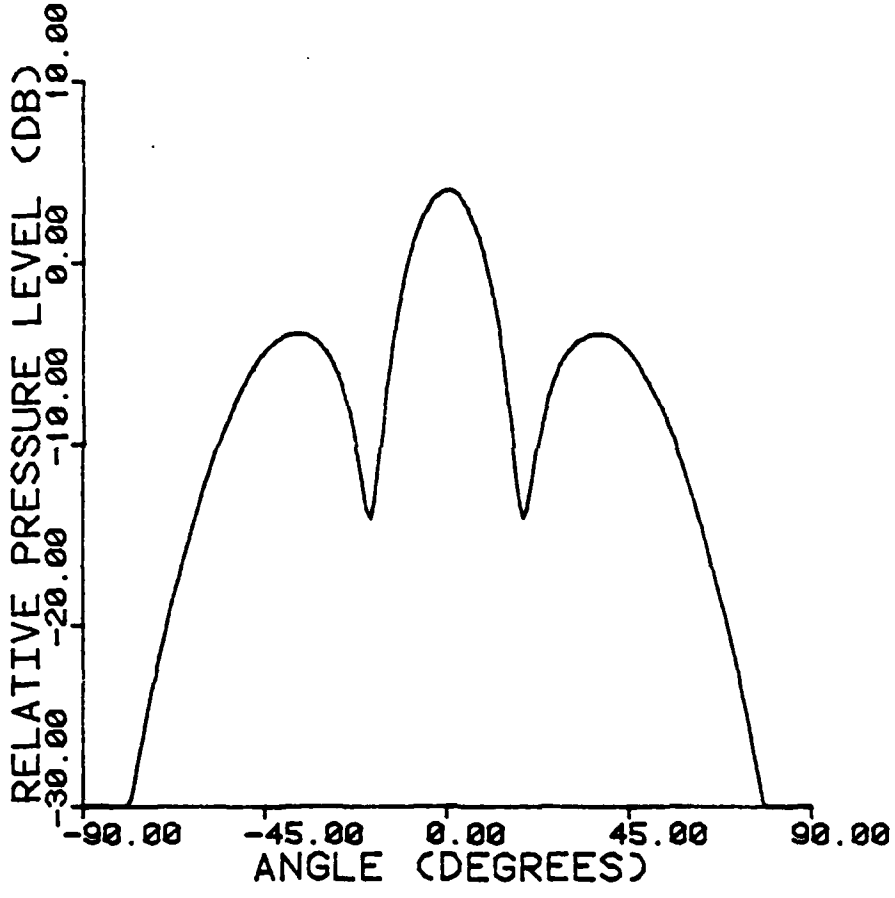

Figure 40. Calculated directivity pattern (concentric rings, L=2) for 40 kHz plane waves. The LC-10 hydrophone is on the axis of symmetry and 0.375" from the grating.

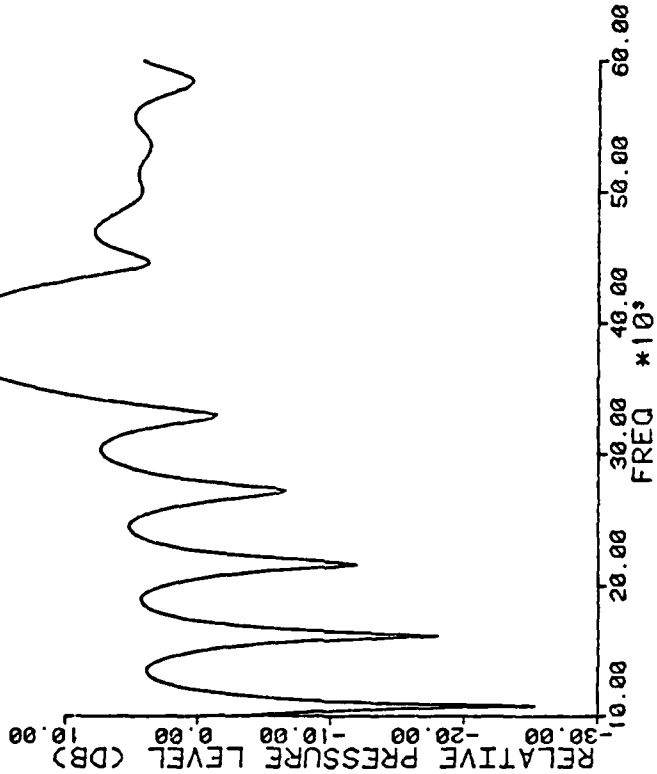

Figure 41. Calculated frequency response of an LC-10 hydrophone 0.375" from the grating (L=8) and on the axis of symmetry for normal incidence plane waves.

CHAPTER V

CONCLUDING REMARKS

5.1 Introduction

In this chapter we summarize the major results of this investigation and present some suggestions for future improvements in the model. In addition another significant application of the technique described in Chapter II is indicated.

5.2 Outline of Model

The research presented in this dissertation has led to the development of a model that will, at least qualitatively, describe the diffraction of sound waves through an aperture in an opaque screen for points of observation within a wavelength of the aperture. To achieve this, the component of the particle velocity normal to the screen is assumed to be the same, in the aperture, as if no screen were present, and zero everywhere else in the plane of the screen. Green's theorem is then used to express the transmitted sound field as the convolution of the assumed normal component of the particle velocity evaluated in the plane of the screen and the Green function appropriate for Neumann boundary conditions on a plane. Using the property that the Fourier transform of the convolution of two functions equals the product of the Fourier transforms of each function, the sound field transmitted through the aperture is found to be proportional to the inverse Fourier transform of the product of the Fourier transform of the Neumann Green function and the Fourier transform of the normal component of the particle velocity in the plane of the

screen. The Fourier transform of the Green function can be evaluated in closed form, while the transform of the normal component of the particle velocity will, in general, have to be evaluated numerically. The inverse Fourier transform is then evaluated numerically. A fast-Fourier-transform algorithm is used to evaluate the forward and inverse Fourier transforms encountered above as computer time is greatly reduced when compared with a direct integral evaluation of the transforms. When considering the diffraction of sound through a grating of concentric rings, it is unnecessary to perform the above calculations for points of observation on the axis of symmetry of the grating. It can be shown that the pressure at a point on the axis of symmetry for incident plane waves can be evaluated by performing the integral in Equation (4.2.1).

When considering diffraction through a grating consisting of straight or circular strips having some extent in a direction normal to the grating, it is necessary to introduce an empirical parameter to take into account the attenuation of the transmitted sound due to geometric shadowing at high angles of incidence.

5.3 Summary of Major Results and Conclusions

It is verified that if one uses a physically appropriate Green function and the suitably modified Kirchhoff boundary conditions [5], then good agreement with experiment is obtained when one considers diffraction of a wave through an aperture where the point of observation is less than one wavelength from the aperture and the aperture is comparable to a wavelength in width. The restriction that the

aperture size be very large compared to a wavelength and that the point of observation be far from the screen encountered when using the traditional Green function (infinite space Green function for outgoing waves) and the Kirchhoff boundary conditions may be relaxed for diffraction of a sound wave through an aperture in an opaque screen if we assume that the normal component of the particle velocity is the same, in the aperture, as if no screen were present and zero everywhere else in the plane of the screen, and use the Neumann Green function. Considering the good results obtained by Stratton and Chu [12] when they applied the vector Smythe-Kirchhoff approximation to a rectangular opening where ka~1, this result should not be too surprising.

Specifically, it is shown in Chapter III that if the gross parabolic structure (due to geometric shadowing) of the directivity pattern is determined by comparison with experiment, excellent agreement is obtained with experiment for diffraction of a plane wave through an aperture consisting of a grating of long, parallel strips having some extent in the direction normal to the grating. In addition, significant discrimination against grazing incidence sound waves is present for a point of observation directly beneath a slit and less than the width of slit from the grating. This property is partly due to geometric shadowing and partly because the normal component of the particle velocity vanishes for sound incident at 90° with respect to the normal to the grating. This property of discrimination against grazing incidence sound is affected, when considering sound emitted by

a localized source, only to the extent that the directivity patterns become slightly broader and more smooth when the source is less than a few wavelengths from the grating.

Also, from considerations presented in Section 3.2.4, it is seen that the primary working assumption made in this research (i.e., for diffraction of a wave through an aperture in an opaque screen, the normal component of the particle velocity is the same, in the aperture, as if no screen were present and zero everywhere else in the plane of the screen) begins to lose validity, for the geometry described in Figure 2, for frequencies below 25 kHz (0.625 wavelengths spacing). This deviation between experiment and theory occurs primarily because the working assumption neglects the detailed scattering of waves in each slit and the interaction between slits.

Finally, for the case of diffraction through a grating of concentric rings having diameters equal to $(2n-1)\ell$, where ℓ is a constant and n equals $1,2,\ldots,L$ (Figure 33), a significant focusing effect is observed when the wavelength of normal incidence waves equals ℓ for points of observation on the axis of symmetry of the grating and less than ℓ inches away from the grating. This effect is relatively insensitive to the distance of the observation point from the grating. If the rings have extent in the direction normal to the grating, then discrimination against grazing incidence sound waves is also present.

5.4 Suggestions for Future Work

Geometric shadowing is an essential constituent in any application utilizing the property of discrimination against grazing incidence sound waves characteristic of a grating of strips having some extent in the direction normal to the grating. Therefore, to use the models developed in the preceding chapters for such applications, a coherent method for calculating the parameter α should be developed. While it is possible to deduce probable values of α from high frequency directivity patterns, such techniques are philosophically unsatisfying with only the limited amount of experimental results available. In the author's opinion a theory applicable to the study of diffraction of a wave through a grating of straight strips can only be developed, without more experimental work, by considering the scattering of waves by an array of square cylinders. Such a method would be costly, time consuming, and not generalizable to the case of diffraction through a grating of concentric rings. Aside from the complications introduced by considering cylinders having a square cross section, the approximations made by Twersky [13] and Klyukin and Chabanov [7] for circular cylinders cannot be made if we consider cylinders having a width comparable to the wavelength of the incident sound and an observation point less than a wavelength away from the grating. As pointed out by Klyukin and Chabanov, computer processing time is likely to become quite long.

However, much useful information can be obtained from the models developed in the preceding chapters for diffraction through an aperture in an opaque screen having no extent in the direction normal to the

screen. Deviations between experiment and theory do not appear to occur for wavelengths comparable to the dimensions of the aperture. If one wishes to reduce any deviations, attention should be given to the detailed perturbation of waves in an aperture. Again, such refinements will be highly dependent on the geometry of the aperture and will not be easily generalizable to other aperture geometries.

Finally, using Equation (2.2.3) one should easily be able to solve exactly and with a minimum of computer time the fundamental problem of radiation from a piston of any configuration in a rigid baffle. For pistons having a simple shape, such as a rectangular piston, the two-dimensional Fourier transform of the piston velocity may be evaluated in closed form. For more complicated geometries the Fourier transform of the piston velocity can be evaluated quickly using a fast-Fourier-transform algorithm. The inverse Fourier transform can then be evaluated by another FFT. As pointed out in Chapter III, one must use an FFT having a large number of integration points for points of observation remote from the piston.

BIBLIOGRAPHY

1. Born, M. and Wolf, E., Principles of Optics, Pergamon Press, New York, (1980).

2. Cooley, J.W., Lewis, P.A.W., and Welch, P.D., "Historical Notes on the Fast Fourier Transform," IEEE Trans. Audio and Electroacoustics, AU15, 76-79, (1967).

3. Freedman, A., "Sound Field of a Rectangular Piston," J. Acoust. Soc. Am., 32, 197-209, (1960).

4. Gradshteyn, I.S. and Ryzhik, I.M., Table of Integrals, Series, and Products, Academic Press, New York, (1980).

5. Jackson, J.D., Classical Electrodynamics, Wiley, New York, (1975).

6. Kinsler, L.E. and Frey, A.R., Fundamentals of Acoustics, Wiley, New York, (1962).

7. Klyukin, I.I. and Chabanov, V.E., "Sound Diffraction by a Plane Grating of Cylinders," Sov. Phys. Acoust., 20, 519-523, (1975).

8. Morse, P.M., Vibration and Sound, Acoustical Society of America, New York, (1976).

9. Quint, R.H., "Acoustic Field of a Circular Piston in the Near Zone," J. Acoust. Soc. Am., 31, 190-191, (1959).

10. Rogers, G.L., "Calculations of Intermediate Fourier Images of a Finite Line Grating on a Digital Computer, with an Application to an Unusual Case," Br. J. Appl. Phys., 14, 657-661, (1963).

11. Skudrzyk, E., The Foundations of Acoustics, Springer-Verlag, New York, (1971).

12. Stratton, J.A. and Chu, L.J., "Diffraction Theory of Electromagnetic Waves," Phys. Rev., 56, 99-107, (1939).

13. Twersky, V., "On Scattering of Waves by the Infinite Grating of Circular Cylinders," IRE Trans. Antennas Propag., AP-10, 737-765, (1962).

14. Williams, E.G., Maynard, J.D., and Skudrzyk, E., "Sound Source Reconstructions Using a Microphone Array," J. Acoust. Soc. Am., 68, 340-344, (1980).

15. Winthrop, J.T. and Worthington, C.R., "Theory of Fresnel Images. I. Plane Periodic Objects in Monochromatic Light," J. Opt. Soc. Am., 55, 373-381, (1965).

16. Zemanek, J., "Beam Behavior within the Nearfield of a Vibrating Piston," J. Acoust. Soc. Am., 49, 181-191, (1971).

APPENDIX A

THE FOURIER TRANSFORM OF THE NEUMANN GREEN FUNCTION FOR A PLANE

A.1 Introduction

In Chapter II, the determination of the transmitted sound field required the evaluation of the two-dimensional Fourier transform of the Neumann Green function for an aperture in the $z = 0$ plane. We perform this transformation below.

A.2 Evaluation of the Transform

We wish to evaluate the Fourier transform of the Neumann Green function

$$G_N(x,y,z) = \frac{e^{ik(x^2+y^2+z^2)^{1/2}}}{2\pi(x^2+y^2+z^2)^{1/2}} \tag{2.2.2}$$

for fixed z. By definition [8],

$$F_2(G_N)=G_N(k_x,k_y,z)= \frac{1}{2\pi}\int_{-\infty}^{\infty}\int_{-\infty}^{\infty}\frac{\exp[ik(x^2+y^2+z^2)^{1/2}]}{(x^2+y^2+z^2)^{1/2}}\, e^{-ik_x x}e^{-ik_y y}dx\,dy\ .$$

Transforming to polar coordinates, this becomes

$$G_N(k_x,k_y,z)= \frac{1}{2\pi}\int_0^{2\pi}\int_0^{\infty}\frac{\exp[ik(r^2+z^2)^{1/2}]}{(r^2+z^2)^{1/2}}\, e^{-ik_\rho r\cos\phi\cos\theta}\, e^{-ik_\rho r\sin\phi\sin\theta} r\,dr\,d\theta$$

$$= \frac{1}{2\pi}\int_0^{\infty}\frac{\exp[ik(r^2+z^2)^{1/2}]}{(r^2+z^2)^{1/2}}\int_0^{2\pi} e^{-ik_\rho r\cos(\phi-\theta)}\,d\theta\,r\,dr$$

$$= \frac{1}{2\pi} \int_0^\infty \frac{\exp[ik(r^2+z^2)^{\frac{1}{2}}]}{(r^2+z^2)^{\frac{1}{2}}} \int_0^{2\pi} e^{-ik_\rho r\sin(\frac{\pi}{2}+\phi-\theta)} d\theta r dr$$

$$= \int_0^\infty \frac{\exp[ik(r^2+z^2)^{\frac{1}{2}}]}{(r^2+z^2)^{\frac{1}{2}}} \left(\frac{1}{2\pi}\right) \int_0^{2\pi} e^{ik_\rho r\sin(\theta-\phi-\frac{\pi}{2})} d\theta r dr \ .$$

Using Gradshteyn and Ryzhik (8.411.1),

$$G_N(k_x,k_y,z) = \int_0^\infty \frac{\exp[ik(r^2+z^2)^{\frac{1}{2}}]}{(r^2+z^2)^{\frac{1}{2}}} J_0(k_\rho r) r dr.$$

Then, from Gradshteyn and Ryzhik (6.737.5) and (6.737.6),

$$G_N(k_x,k_y,z) = \begin{cases} \sqrt{\frac{\pi}{2}}\, z^{\frac{1}{2}}(k^2-k_\rho^2)^{-\frac{1}{4}}[-N_{-\frac{1}{2}}(z\sqrt{k^2-k_\rho^2}) + iJ_{-\frac{1}{2}}(z\sqrt{k^2-k_\rho^2})], & 0<k_\rho<k, z>0 \\ \sqrt{\frac{2}{\pi}}\, z^{\frac{1}{2}}(k_\rho^2-k^2)^{-\frac{1}{4}} K_{\frac{1}{2}}(z\sqrt{k_\rho^2-k^2}), & 0<k<k_\rho, z>0 \end{cases}$$

$$= \begin{cases} \sqrt{\frac{\pi}{2}}\, z^{\frac{1}{2}}(k^2-k_\rho^2)^{-\frac{1}{4}}\left[-\sqrt{\frac{2}{\pi z\sqrt{k^2-k_\rho^2}}}\sin(z\sqrt{k^2-k_\rho^2}) + i\sqrt{\frac{2}{\pi z\sqrt{k^2-k_\rho^2}}}\right. \\ \qquad \left. \times \cos(z\sqrt{k^2-k_\rho^2})\right], & 0<k_\rho<k, z>0 \\ \sqrt{\frac{2}{\pi}}\, z^{\frac{1}{2}}(k_\rho^2-k^2)^{-\frac{1}{4}}\left[\sqrt{\frac{\pi}{2z\sqrt{k_\rho^2-k^2}}}\exp(-z\sqrt{k_\rho^2-k^2})\right], & 0<k<k_\rho, z>0 \end{cases}$$

$$
= \begin{cases} i\dfrac{\exp(iz\sqrt{k^2-k_\rho^2})}{(k^2-k_\rho^2)^{\frac{1}{2}}}, & 0<k_\rho<k, z>0 \\ \dfrac{\exp(-z\sqrt{k_\rho^2-k^2})}{(k_\rho^2-k^2)^{\frac{1}{2}}}, & 0<k<k_\rho, z>0 \end{cases}
$$

$$
= \begin{cases} i\dfrac{\exp[iz(k^2-k_x^2-k_y^2)^{\frac{1}{2}}]}{(k^2-k_x^2-k_y^2)^{\frac{1}{2}}}, & 0<k_x^2+k_y^2<k^2, z>0 \\ \dfrac{\exp[-z(k_x^2+k_y^2-k^2)^{\frac{1}{2}}]}{(k_x^2+k_y^2-k^2)^{\frac{1}{2}}}, & 0<k^2<k_x^2+k_y^2, \ z>0. \end{cases} \qquad (2.2.4)
$$

DISTRIBUTION

Commander (NSEA 0342)
Naval Sea Systems Command
Department of the Navy
Washington, DC 20362 — Copies 1 and 2

Commander (NSEA 9961)
Naval Sea Systems Command
Department of the Navy
Washington, DC 20362 — Copies 3 and 4

Defense Technical Information Center
5010 Duke Street
Cameron Station
Alexandria, VA 22314 — Copies 5 through 10


FILMED
5-8